Effective dispersion in heterogeneous media under random transient flow conditions

Olaf A. Cirpka
Institut für Wasserbau, Universität Stuttgart, Stuttgart, Germany

Sabine Attinger
Swiss Federal Institute of Technology Zurich, Computational Science and Engineering, Zurich, Switzerland

Received 20 December 2002; revised 7 May 2003; accepted 20 June 2003; published 18 September 2003.

[1] Under steady state flow conditions, solute dispersion in heterogeneous porous media is much smaller in the transverse than in the longitudinal direction. This holds particularly for effective dispersion of a plume originating from a point-like injection. The effective dispersion coefficient describes the actual dispersive mixing of solutes in the aquifer. The lack of dispersive transverse mixing may limit considerably natural attenuation of certain contaminants. Temporal fluctuations of the flow direction enhance horizontal transverse dispersion. This has been shown previously for uniform flow and for macrodispersion in stationary media. We present a linear stochastic theory for effective dispersion under quasi-steady state flow conditions with random temporal fluctuations of the mean flow direction. As for macrodispersion, effective transverse dispersion proves to be dominated by transient flow effects. We compare semianalytical results derived from linear theory to those from particle-tracking random-walk simulations for a three-dimensional test case. The parameters of the test case are similar to those obtained at the Borden site, where the mean transverse flow component fluctuated approximately by ±10°. Linear theory and particle simulations agree well. *INDEX TERMS:* 1829 Hydrology: Groundwater hydrology; 1832 Hydrology: Groundwater transport; 1869 Hydrology: Stochastic processes;
KEYWORDS: heterogeneity, effective dispersion, mixing, transient flow, spectral methods

Citation: Cirpka, O. A., and S. Attinger, Effective dispersion in heterogeneous media under random transient flow conditions, *Water Resour. Res.*, *39*(9), 1257, doi:10.1029/2002WR001931, 2003.

1. Introduction

[2] Under steady state flow conditions, solute dispersion in heterogeneous porous media is known as a strongly anisotropic process [*Gelhar and Axness*, 1983; *Dagan*, 1988]. While the longitudinal macrodispersivity increases with travel time by several orders of magnitude, the transverse approaches an asymptotic value only slightly larger than the pore-scale coefficient. These findings also hold for effective dispersion describing actual mixing of solutes in heterogeneous media [*Attinger et al.*, 1999; *Dentz et al.*, 2000a]. For steady state flow, therefore, heterogeneity hardly enhances the mixing of compounds transverse to the mean direction of flow. This is of practical significance in the assessment of natural attenuation: The degradation of certain contaminants requires the presence of strong electron acceptors such as oxygen or nitrogen which are provided as dissolved compounds. Considering a continuously emitting contaminant source, the dissolved electron acceptors will be readily depleted in the source zone. A contaminant plume will evolve, lacking dissolved electron acceptors in its center. While longitudinal mixing is dominant at the downstream front of the expanding plume, slow transverse dispersive mixing will determine the large-time, quasi-steady state behavior: Oxygen or nitrate must be mixed laterally into the plume. That is, for plumes originating from a continuous source, transverse dispersive mixing determines the effective reaction rates and the length approached by the plume in the large-time limit; the smaller the effective transverse dispersion, the longer the plume [*Cirpka et al.*, 1999; *Thornton et al.*, 2001; *Thullner et al.*, 2002].

[3] Steady state flow conditions, however, are seldom observed in natural aquifers. At many sites, the direction of flow changes over time due to temporal variations in the hydrological regime. Figure 1 illustrates schematically the impact of transient flow on the transport of a solute cloud. The trajectory of the plume center is shown as solid line. Initially, there is an upward mean flow component, and the plume spreads into the direction that is longitudinal at that time. Then the direction of flow changes, and what used to be the longitudinal direction is now the transverse one. In the subsequent time period the plume spreads into the new longitudinal direction which becomes the transverse direction in the next period, and so forth. In Figure 1 the overall flow direction is marked as dashed line. In the temporal average, apparently, a significant portion of dispersion acts in the overall transverse direction.

[4] *Kinzelbach and Ackerer* [1986] and *Goode and Konikow* [1990] analyzed dispersion in a uniform flow field with temporal fluctuations in the direction of the hydraulic

0043-1397/03/2002WR001931

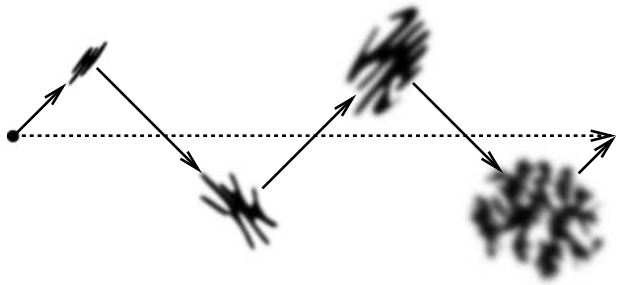

Figure 1. Effect of changes in the mean flow direction on transverse dispersion.

gradient, deriving simple time-averaged expressions. Recently, *Schirmer et al.* [2001] showed that enhanced transverse dispersion coefficients may be used to account for the effect of transient flow on mixing in bio-reactive transport. While these approaches are simple to apply, they imply that the asymptotic macrodispersion coefficients are valid at all times and that they describe the actual mixing of interacting compounds. Neither assumption withstands a critical analysis.

[5] For stationary heterogeneous media, *Kabala and Sposito* [1991], *Rehfeldt and Gelhar* [1992], *Dagan et al.* [1996], and *Zhang and Neuman* [1996] derived first-order expressions of macrodispersion accounting for temporal variability in the velocity fields. *Kabala and Sposito* [1991] assumed that the spatial cross-covariance between the velocities at two times depends on the time lag rather than the definite time points, which implies the velocities to be a second-order stationary random process in time. However, they did not derive expressions for the velocity covariance itself. *Rehfeldt and Gelhar* [1992] assumed a random mean hydraulic gradient characterized exclusively by its temporal covariance function. These authors parameterized the impact of the uncertain mean hydraulic gradient on solute transport as an additional dispersive term that they treated separately from dispersion caused by spatial fluctuations in the log conductivity. *Zhang and Neuman* [1996] and *Dagan et al.* [1996], by contrast, stated that the cross-effects of temporal and spatial fluctuations do not average out. These authors assumed deterministic temporal fluctuations of the mean hydraulic gradient, derived closed-form expressions for the velocity covariance and substituted those into macrodispersion expressions for strictly advective transport. In all of these studies, like in the present study, the storativity of the aquifer was neglected so that groundwater flow was assumed to react instantaneously to changes in the mean hydraulic gradient. *Kavvas and Karakas* [1996] and *Li and Graham* [1999], in contrast, considered spatiotemporal fluctuations in flow fields with nonzero divergence caused by groundwater storage or recharge. The analysis of *Kavvas and Karakas* [1996] was extended by *Wood and Kavvas* [1999] to include linear reactions.

[6] All authors cited above analyzed classical macrodispersion, that is, the temporal development of second central spatial moments of the ensemble-averaged concentration. Macrodispersion merges the rate of change of two types of information: the expected second central moment of plumes in single realizations, and the uncertainty in detecting the plume center from realization to realization [*Kitanidis*, 1988]. Half the rate of change of the first quantity is referred to as effective dispersion [*Rajaram and Gelhar*, 1993, 1995; *Attinger et al.*, 1999; *Dentz et al.*, 2000a, 2000b], whereas in the Lagrangian framework the second quantity is known as two-particle covariance of displacement [*Fiori and Dagan*, 2000]. For a point-like injection and small pore-scale dispersion coefficients, macrodispersion and effective dispersion differ significantly at early times. Under these conditions, macrodispersion primarily quantifies the uncertainty in tagging the plume center and hardly describes how plumes in single realizations spread [*Dentz et al.*, 2000a; *Fiori and Dagan*, 2000]. The wider the initial plume is extended in the direction perpendicular to the mean flow, the faster the longitudinal effective dispersion coefficient approaches the macrodispersion coefficient [*Dentz et al.*, 2000b]. At the limit of an infinitely wide plume the two types of longitudinal dispersion coefficients become identical. It may be noteworthy that *Andricevic and Cvetkovic* [1998] referred to effective dispersion as relative dispersion and to macrodispersion as absolute dispersion [see also *Chatwin and Sullivan*, 1979; *Fiori*, 2001].

[7] *Cirpka* [2002] demonstrated that the effective dispersion coefficient for a point-like injection is an adequate measure of actual dispersive mixing, even for wide plumes. In order to facilitate reactions between compounds that were separated in the initial state, mixing must occur on the scale of single pores. For these reactions, at first, it is irrelevant how the second central moments of a wide plume increase, since these moments primarily describe the irregularity of the plume shape. By contrast, the point-related effective dispersion coefficients describe the expected area influencing the concentrations at a point. Hence, for mixing-controlled reactive transport, the effective dispersion coefficient for a point-like injection quantifies dispersive mixing, whereas additional spreading of a large plume is quantified by the corresponding covariance of first moments [*Cirpka and Kitanidis*, 2000; *Cirpka*, 2002]. In the present study, we will use the term "effective dispersion" only for the case of a point-like injection.

[8] Like the macrodispersivities, the effective dispersivities show strong anisotropy: Under steady state flow conditions, in typical heterogeneous formations, effective dispersion in the transverse direction may approach a value that is at most a single order of magnitude larger than the corresponding pore-scale coefficient, whereas the longitudinal effective dispersivity approaches, at very large times, the value of the asymptotic macrodispersivity which is by several orders of magnitude larger than the pore-scale value. In the present study, we analyze effective dispersion under transient flow conditions. In particular, we investigate how fluctuations in the mean transverse flow component enhance transverse effective dispersion. As outlined above, we believe this to be important in assessing certain scenarios of natural attenuation.

[9] From the analyses of uniform flow [*Kinzelbach and Ackerer*, 1986; *Goode and Konikow*, 1990] and macrodispersion in heterogeneous media [*Rehfeldt and Gelhar*, 1992; *Dagan et al.*, 1996; *Zhang and Neuman*, 1996] one might expect a partial reorientation of longitudinal effective dispersion components into the transverse direction. For effective dispersion the process of spatial reorientation might be important also in a second sense. As already

mentioned, the time for effective dispersion to approach the values of macrodispersion decreases with increasing width of the plume [*Dentz et al.*, 2000b]. In the scenario illustrated in Figure 1 the spatial reorientation makes the plume starting with a larger width in each period of constant mean flow direction. Therefore transient flow may not only increase the values of transverse effective dispersivity but also make effective dispersion catching up significantly faster with macrodispersion than under steady state flow conditions. We have observed such effects in particle-tracking random-walk simulations in cases with large temporal fluctuations of the mean hydraulic gradient. These higher-order effects, however, are not included in the first-order stochastic analysis presented in this paper. We restrict therefore the present study to cases with small fluctuations of the mean hydraulic gradient.

2. Theory

2.1. Quasi-Steady State Flow in Heterogeneous Media

[10] Consider a spatially stationary log conductivity field $Y(\mathbf{x}) = \ln(K(\mathbf{x}))$ with locally isotropic hydraulic conductivity $K(\mathbf{x})$. The log conductivity field is described by second-order statistics:

$$\exp\left(\langle Y(\mathbf{x})\rangle_{\mathbf{x}}\right) = K_g \forall \mathbf{x} \tag{1}$$

$$\langle Y'(\mathbf{x})Y'(\mathbf{x}+\mathbf{h})\rangle_{\mathbf{x}} = R_{Y'Y'}(\mathbf{h}) \forall \mathbf{x} \tag{2}$$

in which $\mathbf{x}$ is the vector of spatial coordinates, $\langle\rangle_{\mathbf{x}}$ denotes the expected-value operator for quantities exhibiting random spatial fluctuations, $Y'(\mathbf{x}) = Y(\mathbf{x}) - \langle Y(\mathbf{x})\rangle_{\mathbf{x}}$ is the deviation from the expected value, K_g is the uniform geometric mean of the hydraulic conductivity, and $R_{Y'Y'}(\mathbf{h})$ is the auto-covariance of the log conductivity fluctuations with separation vector $\mathbf{h}$.

[11] The distribution of hydraulic heads $\phi(\mathbf{x}, t)$ at time t is determined by the well-known groundwater flow equation:

$$S_0 \frac{\partial \phi}{\partial t} - \nabla \cdot (K \nabla \phi) = 0 \tag{3}$$

subject to initial and boundary or auxiliary conditions. S_0 is the specific storativity. In confined, sandy aquifers, the value of S_0 is on the order of 10^{-6}. For gradual temporal variations of the mean hydraulic gradient in fairly permeable formations, it is reasonable to neglect the storage term, that is, to assume quasi-steady state conditions:

$$\nabla \cdot (K \nabla \phi) = 0 \tag{4}$$

subject to time-dependent boundary or auxiliary conditions. For the latter, we assume a uniform mean negative hydraulic gradient $\mathbf{J}(t)$:

$$\langle \nabla \phi(\mathbf{x}, t)\rangle_{\mathbf{x}} = -\mathbf{J}(t) \forall \mathbf{x} \tag{5}$$

[12] In many applications, the temporal fluctuations of the mean hydraulic gradient will be deterministic, simply because it can be measured. We will come back to the deterministic case in section 2.6. First, however, we consider the temporal fluctuations as random process. Random fluctuations may be caused by an irregular hydrological regime. They can also be interpreted as a random initial time point at which the solute is released into the aquifer when the temporal fluctuations follow a regular seasonal trend. As will be seen later, the assumption of random temporal fluctuations is computationally advantageous over the deterministic case. We consider the mean hydraulic gradient as a random stationary time process characterized by second-order statistics:

$$\langle \mathbf{J}(t)\rangle_t = \bar{\mathbf{J}} \; \forall t \tag{6}$$

$$\left\langle \mathbf{J}'(t)\mathbf{J}'^T(t+\tau)\right\rangle_t = \mathbf{R}_{\mathbf{J}'\mathbf{J}'^T}(\tau) \tag{7}$$

in which $\langle\rangle_t$ denotes the expected-value operator for quantities exhibiting random temporal fluctuations, and $\mathbf{J}'(t) = \mathbf{J}(t) - \bar{\mathbf{J}}$ is the deviation from the expected value. Throughout this paper, vectors such as the mean hydraulic gradient $\mathbf{J}$ are considered column vectors. $\mathbf{J}^T$ is the transpose of $\mathbf{J}$ and thus a row vector. Applying standard rules of matrix multiplication, $\mathbf{J}'(t)\mathbf{J}'^T(t+\tau)$ is a dyad, that is, a matrix with entries $J_i'(t)\, J_j'(t+\tau)$. In the following, we will also encounter scalar products of some vectors $\mathbf{a}$ and $\mathbf{b}$ which may be written in the notation $\mathbf{a}^T\mathbf{b} = \mathbf{a} \cdot \mathbf{b}$.

[13] The log conductivity varies in space and the mean hydraulic gradient in time, so that the two varying quantities are uncorrelated:

$$\langle Y'(\mathbf{x})\mathbf{J}'(t)\rangle = 0 \tag{8}$$

[14] Introducing small perturbations into the quasi-steady state groundwater flow equation, equation (4), and linearizing $\exp(Y'(\mathbf{x}))$ by $1+Y'(\mathbf{x})$ yields:

$$\nabla \cdot \left(K_g(1 + Y'(\mathbf{x}))(\bar{\mathbf{J}} + J'(t) - \nabla\phi'(\mathbf{x}, t))\right) = 0 \tag{9}$$

Subtracting the expected value from equation (9), considering that $\mathbf{J}(t)$ is spatially uniform, and dropping the terms of second order in space, yields the stochastic groundwater flow equation:

$$-\nabla^2\phi'(\mathbf{x}, t) + \nabla Y'(\mathbf{x}) \cdot \bar{\mathbf{J}} + \nabla Y'(\mathbf{x}) \cdot \mathbf{J}'(t) = 0 \tag{10}$$

which is of first order in both space and time. In their analysis, *Rehfeldt and Gelhar* [1992] dropped the product $\nabla Y'(\mathbf{x}) \cdot J'(t)$, while we keep it. As will be seen, this has consequences for the evaluation of the velocity spectrum and the effective dispersion tensor. We transfer equation (10) into the spatial Fourier domain:

$$4\pi^2\mathbf{s}^T\mathbf{s}\tilde{\phi}'(\mathbf{s}, t) + 2\pi i\mathbf{s}^T\bar{\mathbf{J}}\tilde{Y}'(\mathbf{s}) + 2\pi i\mathbf{s}^T\tilde{\mathbf{J}}'(t)\tilde{Y}'(s) = 0 \tag{11}$$

in which $\mathbf{s}$ is the spatial wave number, and quantities marked by a tilde are Fourier transforms defined here in the following form [*Press et al.*, 1992, chap. 12]:

$$\tilde{f}(\mathbf{s}, t) = \int_{\infty} f(\mathbf{x}, t) \exp(-2\pi i\mathbf{x}^T\mathbf{s}) d\mathbf{x} \tag{12}$$

$$f(\mathbf{x}, t) = \int_{\infty} \tilde{f}(\mathbf{s}, t) \exp(2\pi i\mathbf{x}^T\mathbf{s}) d\mathbf{s} \tag{13}$$

From equation (11), we can relate the Fourier transform of the hydraulic-head perturbations and their spatial derivative to the Fourier transforms of the log conductivity and mean hydraulic gradient fluctuations:

$$\tilde{\phi}'(\mathbf{s},t) = -\frac{2\pi i \mathbf{s}^T \bar{\mathbf{J}} \tilde{Y}'(\mathbf{s}) + 2\pi i \mathbf{s}^T \tilde{\mathbf{J}}'(t) \tilde{Y}'(s)}{4\pi^2 \mathbf{s}^T \mathbf{s}} \tag{14}$$

$$\widetilde{\nabla\phi}'(\mathbf{s},t) = \frac{\mathbf{s}\mathbf{s}^T \bar{\mathbf{J}} \tilde{Y}'(\mathbf{s}) + \mathbf{s}\mathbf{s}^T \tilde{\mathbf{J}}'(t) \tilde{Y}'(s)}{\mathbf{s}^T \mathbf{s}} \tag{15}$$

Introducing first-order perturbations into Darcy's law leads to the following expression:

$$\mathbf{q}(\mathbf{x},t) = K_g(1 + Y'(\mathbf{x}))(\bar{\mathbf{J}} + \mathbf{J}'(t) - \nabla\phi'(\mathbf{x},t)) \tag{16}$$

in which $\mathbf{q}(\mathbf{x}, t)$ is the specific-discharge vector. The first-order mean of the specific discharge is obtained by dropping higher-order terms and taking the expected value:

$$\langle \mathbf{q} \rangle^{(1)} = \langle \mathbf{q} \rangle^{(0)} = K_g \bar{\mathbf{J}} \tag{17}$$

Subtracting $\langle \mathbf{q} \rangle^{(1)}$ from equation (16) and dropping terms of second order in space yields:

$$\mathbf{q}'(\mathbf{x},t) = K_g(\mathbf{J}'(t) - \nabla\phi'(\mathbf{x},t) + Y'(\mathbf{x})(\bar{\mathbf{J}} + \mathbf{J}'(t))) \tag{18}$$

Again, we keep the mixed term $Y'(\mathbf{x})\mathbf{J}'(t)$ which has been dropped by *Rehfeldt and Gelhar* [1992]. Transferring equation (18) into the spectral domain and considering equation (15) yields the Fourier transform $\tilde{\mathbf{q}}'(\mathbf{s}, t)$ of the specific-discharge fluctuations $\mathbf{q}'(\mathbf{x}, t)$:

$$\tilde{\mathbf{q}}'(\mathbf{s},t) = K_g\left(\delta(\mathbf{s})\tilde{\mathbf{J}}'(t) + \left(\bar{\mathbf{J}} + \tilde{\mathbf{J}}'(t) - \frac{\mathbf{s}\mathbf{s}^T}{\mathbf{s}^T\mathbf{s}}\left(\bar{\mathbf{J}} + \tilde{\mathbf{J}}'(t)\right)\right)\tilde{Y}'(\mathbf{s})\right) \tag{19}$$

[15] Multiplying the Fourier transform of the specific discharge $\tilde{\mathbf{q}}'(\mathbf{s}, t)$ at a given time t with its transpose of the complex conjugate $\tilde{\mathbf{q}}'^{*\,T}(\mathbf{s}, t')$ at a different time t' and taking expected values leads to the space spectrum/time covariance of specific-discharge fluctuations $\mathcal{S}_{\mathbf{q}'\mathbf{q}'}(\mathbf{s}, \tau)$:

$$\begin{aligned}\mathcal{S}_{\mathbf{q}'\mathbf{q}'^T}(\mathbf{s},\tau) = K_g^2\Bigg(&\left(\bar{\mathbf{J}} - \frac{\mathbf{s}\mathbf{s}^T\bar{\mathbf{J}}}{\mathbf{s}^T\mathbf{s}}\right)\left(\bar{\mathbf{J}} - \frac{\mathbf{s}\mathbf{s}^T\bar{\mathbf{J}}}{\mathbf{s}^T\mathbf{s}}\right)^T S_{Y'Y'}(\mathbf{s}) \\ &+ \delta(\mathbf{s})\mathbf{R}_{\mathbf{J}'\mathbf{J}'^T}(\tau) + \mathbf{R}_{\mathbf{J}'\mathbf{J}'^T}(\tau) S_{Y'Y'}(\mathbf{s}) \\ &- \left(\frac{\mathbf{s}\mathbf{s}^T}{\mathbf{s}^T\mathbf{s}}\mathbf{R}_{\mathbf{J}'\mathbf{J}'^T}(\tau) + \mathbf{R}_{\mathbf{J}'\mathbf{J}'^T}(\tau)\frac{\mathbf{s}\mathbf{s}^T}{\mathbf{s}^T\mathbf{s}}\right) S_{Y'Y'}(\mathbf{s}) \\ &+ \frac{\mathbf{s}\mathbf{s}^T\mathbf{R}_{\mathbf{J}'\mathbf{J}'^T}(\tau)\mathbf{s}\mathbf{s}^T}{(\mathbf{s}^T\mathbf{s})^2} S_{Y'Y'}(\mathbf{s})\Bigg)\end{aligned} \tag{20}$$

in which $\tau = t - t'$ is the time lag. The expressions in equation (20) contain three principal components depending on (1) spatial fluctuations alone, (2) temporal fluctuations alone, and (3) both spatial and temporal fluctuations. In steady state flows, only the time-invariant terms occur. *Rehfeldt and Gelhar* [1992] added only the term depending exclusively on temporal fluctuations. As we will show later, the latter contribution has no effect on effective dispersion. The impact of transient flow on effective dispersion is given by the mixed terms which were neglected by *Rehfeldt and Gelhar* [1992].

2.2. Conservative Transport

[16] Consider transport of a conservative solute in an infinite domain. In the initial state, we assume the solute mass of unity concentrated in a single point at $\mathbf{x} = 0$:

$$\frac{\partial c}{\partial t} + (\langle \mathbf{v} \rangle + \mathbf{v}') \cdot \nabla c - \nabla \cdot (\mathbf{D}\nabla c) = 0 \tag{21}$$

$$c(\mathbf{x}, t = 0) = \delta(\mathbf{x}) \tag{22}$$

$c(\mathbf{x}, t)$ is the concentration of the solute. The mean seepage velocity $\langle \mathbf{v} \rangle = \langle \mathbf{q} \rangle^{(1)}/\theta$ is given by equation (17) and the space-time perturbation $\mathbf{v}'(\mathbf{x}, t) = \mathbf{q}'(\mathbf{x}, t)/\theta$ by equation (18). $\mathbf{D}$ and θ are the pore-scale dispersion tensor and the porosity, respectively, both assumed uniform and time-invariant. We are aware that pore-scale dispersion coefficients vary with the local velocity and therefore with space and time. However, going through the formalism outlined in the following, it turns out that spatiotemporal fluctuations of pore-scale dispersion have, to the order considered in the present study, no impact on macrodispersion and effective dispersion. This is consistent to previous findings [*Gelhar*, 1993]. The uniform pore-scale dispersion tensor used in the following analysis represents therefore the spatiotemporal average of the fluctuating tensor.

[17] In the analysis of macroscopic transport, we adopt the formalism outlined by *Attinger et al.* [1999] and *Dentz et al.* [2000a]. The only difference to the study of *Dentz et al.* [2000a] lies in the random time-dependence of the seepage velocity $\mathbf{v}(t)$ requiring some modifications of the approach derived for steady state flow. We express the velocity fluctuations $\mathbf{v}'(\mathbf{x}, t)$ and the concentration $c(\mathbf{x}, t)$ by their Fourier transforms $\tilde{\mathbf{v}}'(\mathbf{s}, t)$ and $\tilde{c}(\mathbf{s}, t)$. Transferring the transport equation, equation (21), and the initial condition, equation (22), into the spectral domain leads to:

$$\begin{aligned}&\frac{\partial \tilde{c}(\mathbf{s},t)}{\partial t} + 2\pi i \mathbf{s}^T \langle \mathbf{v} \rangle \tilde{c}(\mathbf{s},t) + 4\pi^2 \mathbf{s}^T \mathbf{D}\mathbf{s}\tilde{c}(\mathbf{s},t) \\ &\qquad = -2\pi i \int_\infty \mathbf{s}^T \tilde{\mathbf{v}}'(\mathbf{s}',t)\tilde{c}(\mathbf{s}-\mathbf{s}',t))d\mathbf{s}'\end{aligned} \tag{23}$$

$$\tilde{c}(\mathbf{s}, t = 0) = 1 \tag{24}$$

[18] The transport equation in the Fourier domain, equation (23), is a differential equation of $\tilde{c}(\mathbf{s}, t)$, to be solved independently for each value of $\mathbf{s}$, with the initial condition, equation (24). This system can be expressed in a corresponding integral form:

$$\tilde{c}(\mathbf{s},t) = \tilde{c}_0(\mathbf{s},t) - \int_0^t \frac{\tilde{c}_0(\mathbf{s},t)}{\tilde{c}_0(\mathbf{s},t')} 2\pi i \cdot \int_\infty \mathbf{s}^T \tilde{\mathbf{v}}'(\mathbf{s}',t'))\tilde{c}(\mathbf{s}-\mathbf{s}',t')d\mathbf{s}'dt' \tag{25}$$

in which $\tilde{c}_0(\mathbf{s}, t)$ is the Fourier transform of the concentration distribution $c_0(\mathbf{x}, t)$ for a homogeneous flow field, i.e., $\mathbf{v}'(\mathbf{x}, t) = \mathbf{0}$. The analytical expression of $\tilde{c}_0(\mathbf{s}, t)$ is:

$$\tilde{c}_0(\mathbf{s},t) = \exp\left(-\left(2\pi i \mathbf{s}^T \langle \mathbf{v} \rangle + 4\pi^2 \mathbf{s}^T \mathbf{D}\mathbf{s}\right)t\right) \tag{26}$$

[19] From equation (25), we can construct a series of $\tilde{c}(\mathbf{s}, t)$ in $\tilde{\mathbf{v}}'(\mathbf{s}', t)$:

$$\tilde{c}(\mathbf{s},t) = \tilde{c}_0(\mathbf{s},t) - 2\pi i \int_0^t \frac{\tilde{c}_0(\mathbf{s},t)}{\tilde{c}_0(\mathbf{s},t')}\mathbf{s}^T \cdot \int_\infty \tilde{\mathbf{v}}'(\mathbf{s}',t'))\tilde{c}_0(\mathbf{s}-\mathbf{s}',t')dt'd\mathbf{s}'$$
$$- 4\pi^2 \int_\infty \int_\infty \int_0^t \int_0^{t'} \frac{\tilde{c}_0(\mathbf{s},t)}{\tilde{c}_0(\mathbf{s},t')}\frac{\tilde{c}_0(\mathbf{s}-\mathbf{s}',t')}{\tilde{c}_0(\mathbf{s}-\mathbf{s}',t'')}\tilde{c}_0(\mathbf{s}-\mathbf{s}'-\mathbf{s}'',t'')\mathbf{s}^T$$
$$\cdot \int_\infty \int_\infty \tilde{\mathbf{v}}'(\mathbf{s}',t')\tilde{\mathbf{v}}'^T(\mathbf{s}'',t'')(\mathbf{s}-\mathbf{s}')dt''dt'd\mathbf{s}''d\mathbf{s}' + \ldots \quad (27)$$

which is truncated here after the second-order term. When taking expected values, we apply the following rule regarding the product of velocity fluctuations:

$$\langle \tilde{\mathbf{v}}'(\mathbf{s}',t)\tilde{\mathbf{v}}'^T(\mathbf{s}'',t')\rangle = \langle \tilde{\mathbf{v}}'(\mathbf{s}',t)\tilde{\mathbf{v}}'^{*T}(-\mathbf{s}'',t')\rangle$$
$$= \mathcal{S}_{\mathbf{v}'\mathbf{v}'^T}(\mathbf{s}',t-t')\delta(\mathbf{s}'+\mathbf{s}'') \quad (28)$$

in which $\tilde{\mathbf{v}}'^*$ is the complex conjugate of $\tilde{\mathbf{v}}'$ and $\mathcal{S}_{\mathbf{v}'\mathbf{v}'^T}(\mathbf{s}', t)$ is the spatial spectrum/temporal covariance function of seepage velocity fluctuations. Assuming a uniform distribution of the porosity θ, the space spectrum/time covariance $\mathcal{S}_{\mathbf{v}'\mathbf{v}'^T}(\mathbf{s}', t)$ is given by:

$$\mathcal{S}_{\mathbf{v}'\mathbf{v}'^T}(\mathbf{s}',t) = \frac{\mathcal{S}_{\mathbf{q}'\mathbf{q}'^T}(\mathbf{s}',t)}{\theta^2} \quad (29)$$

where $\mathbf{S}_{\mathbf{q}'\mathbf{q}'^T}(\mathbf{s}',t)$ is evaluated by equation (20).

[20] Taking the expected value of equation (27) yields the Fourier transform $\langle\tilde{c}(\mathbf{s}, t)\rangle$ of the ensemble-averaged concentration $\langle c(\mathbf{s}, t)\rangle$:

$$\langle\tilde{c}(\mathbf{s},t)\rangle = \tilde{c}_0(\mathbf{s},t) - 4\pi^2 \int_\infty \int_0^t \int_0^{t'} \frac{\tilde{c}_0(\mathbf{s},t)\ \tilde{c}_0(\mathbf{s}-\mathbf{s}',t')}{\tilde{c}_0(\mathbf{s},t')\,\tilde{c}_0(\mathbf{s}-\mathbf{s}',t'')}\tilde{c}_0(\mathbf{s},t'')$$
$$\cdot \mathbf{s}^T\mathcal{S}_{\mathbf{v}'\mathbf{v}'^T}(\mathbf{s}',t'-t'')(\mathbf{s}-\mathbf{s}')dt''dt'd\mathbf{s}' \quad (30)$$

[21] Conceptually, the ensemble-averaged concentration $\langle c(\mathbf{x}, t)\rangle$ is obtained by considering all realizations of the log conductivity field and the history of mean gradient fluctuations meeting the prescribed statistical moments, performing a transport calculation in each of those realizations, and taking the average of the concentration over all realizations. Thus $\langle c(\mathbf{x}, t)\rangle$ is affected by both the spatial uncertainty in the log conductivity and the temporal uncertainty in the mean hydraulic gradient.

2.3. Dispersion Coefficients

[22] As shown in Appendix A, the spatial moments of the expected concentration $\langle c(\mathbf{x}, t)\rangle$ can be calculated from the derivatives of its Fourier transform $\langle\tilde{c}(\mathbf{s}, t)\rangle$ at the origin, $\mathbf{s} = \mathbf{0}$. We denote the matrix of second central moments of the expected concentration by $\mathbf{M}^c_{\mathbf{x}\mathbf{x}T}(\langle c(\mathbf{x}, t)\rangle)$. Half the rate of change of $\mathbf{M}^c_{\mathbf{x}\mathbf{x}T}(\langle c(\mathbf{x}, t)\rangle)$ is known as the classical macrodispersion tensor, referred to as ensemble dispersion tensor by *Dentz et al.* [2000a]. As discussed in detail by *Attinger et al.* [1999] and *Dentz et al.* [2000a], the order of taking the expected value and evaluating the second central moments is significant. By first taking the moments and subsequently the expected value, one arrives at the expected value of the matrix of second central moments $\langle\mathbf{M}^c_{\mathbf{x}\mathbf{x}T}(c(\mathbf{x}, t))\rangle$. The corresponding steps of calculation are reviewed in Appendix A. Half the rate of change of $\langle\mathbf{M}^c_{\mathbf{x}\mathbf{x}T}(c(\mathbf{x}, t))\rangle$ is the effective dispersion tensor, here derived for a point-like injection in a heterogeneous domain under random fluctuations of the mean hydraulic gradient. Substituting equation (26) into equations (A3) and (A5), considering the incompressibility of the flow field, $\mathbf{s}'^T\tilde{\mathbf{v}}'(\mathbf{s}', t) = 0$, and taking half the derivatives yields:

$$\mathbf{D}^*(t) = \frac{1}{2}\frac{\partial\mathbf{M}^c_{\mathbf{x}\mathbf{x}^T}(\langle c(\mathbf{x},t)\rangle)}{\partial t}$$
$$= \mathbf{D} + \int_\infty \int_0^t \frac{\tilde{c}_0(-\mathbf{s},t)}{\tilde{c}_0(-\mathbf{s},t')}\mathcal{S}_{\mathbf{v}'\mathbf{v}'^T}(\mathbf{s},t-t')dt'd\mathbf{s}$$
$$= \mathbf{D} + \int_\infty \int_0^t \exp\big(\big(2\pi i\mathbf{s}^T\langle\mathbf{v}\rangle - 4\pi^2\mathbf{s}^T\mathbf{D}\mathbf{s}\big)\tau\big)\mathcal{S}_{\mathbf{v}'\mathbf{v}'^T}(\mathbf{s},\tau)d\tau d\mathbf{s} \quad (31)$$

$$\mathbf{D}^e(t) = \frac{1}{2}\frac{\partial\langle\mathbf{M}^c_{\mathbf{x}\mathbf{x}^T}(c(\mathbf{x},t))\rangle}{\partial t}$$
$$= \mathbf{D}^*(t) - \int_\infty \int_0^t \mathcal{S}_{\mathbf{v}'\mathbf{v}'^T}(\mathbf{s},t-t')\tilde{c}_0(-\mathbf{s},t)\tilde{c}_0(\mathbf{s},t')dt'd\mathbf{s}$$
$$= \mathbf{D}^*(t) - \int_\infty \exp\big(-8\pi^2\mathbf{s}^T\mathbf{D}\mathbf{s}t\big)$$
$$\cdot \int_0^t \exp\big(\big(4\pi^2\mathbf{s}^T\mathbf{D}\mathbf{s} + 2\pi i\mathbf{s}^T\langle\mathbf{v}\rangle\big)\tau\big)\mathcal{S}_{\mathbf{v}'\mathbf{v}'^T}(\mathbf{s},\tau)d\tau d\mathbf{s} \quad (32)$$

These expressions are formally identical to those of *Dentz et al.* [2000a] for the case of steady state flow. However, the underlying spectrum/covariance $\mathcal{S}_{\mathbf{v}'\mathbf{v}'^T}(\mathbf{s},\tau)$ differs from the steady state case. Conceptually, the macrodispersion tensor $\mathbf{D}^*(t)$ in the present study is affected by the uncertainty in the mean hydraulic gradient fluctuations. The dispersion tensors for deterministic temporal fluctuations, or a single realization of the temporal fluctuations, differ from our results. In particular, the macrodispersion tensor $\mathbf{D}^*(t)$ for a single realization of the temporal fluctuations is smaller than given in equation (31), and the corresponding effective dispersion tensor $\mathbf{D}^e(t)$ reflects the actual mean hydraulic gradient $\mathbf{J}(t)$ at a given time t. For the special case of sinusoidal fluctuations, our result of the effective dispersion tensor $\mathbf{D}^e(t)$ is the average over all phase angles. Our expression for macrodispersion, equation (31), is identical to equation (18) of *Kabala and Sposito* [1991].

2.4. Closed-Form Expressions and Approximate Solutions

[23] *Dentz* [2000] presented closed-form expressions for the longitudinal and transverse components of $\mathbf{D}^*(t)$ and $\mathbf{D}^e(t)$ under steady state flow conditions assuming a Gaussian covariance function $R_{Y'Y'}(\mathbf{h})$ of the log conductivity fluctuations. We extend these results for temporal fluctuations in the mean hydraulic gradient $\mathbf{J}$. In general, we need to consider four contributions to the macrodispersion tensor:

$$\mathbf{D}^*(t) = \mathbf{D} + \mathbf{D}^*_{\delta(Y)}(t) + \mathbf{D}^*_{\delta(t)}(t) + \mathbf{D}^*_{mix}(t) \quad (33)$$

in which $\mathbf{D}$ is the pore-scale dispersion tensor, $\mathbf{D}^*_{\delta(Y)}(t)$ the contribution from spatial variability of the log conductivity alone, and $\mathbf{D}^*_{\delta(t)}(t)$ from uncertainty in the mean hydraulic gradient alone, whereas $\mathbf{D}^*_{mix}(t)$ includes the mixed terms of log conductivity and hydraulic gradient fluctuations. The three macroscopic terms are related to the corresponding

terms in the space spectrum/time covariance $\mathcal{S}_{\mathbf{v}'\mathbf{v}'^T}(\mathbf{s},\tau)$ of the velocity fluctuations. $\mathbf{D}^*_{\delta(Y)}(t)$ is well-known from the analysis of macrodispersion in steady state flows [*Gelhar and Axness*, 1983; *Dagan*, 1988]. The contribution $\mathbf{D}^*_{\delta(t)}(t)$, analyzed by *Rehfeldt and Gelhar* [1992], is given by integration of the temporal covariance matrix $\mathbf{R}_{\mathbf{J}'\mathbf{J}'}(\tau)$ of the mean gradient fluctuations:

$$\mathbf{D}^*_{\delta(t)}(t) = \frac{K_g^2}{\theta^2}\int_0^t \mathbf{R}_{\mathbf{J}'\mathbf{J}'^T}(\tau)d\tau \tag{34}$$

which is easy to derive. We focus our analysis on the mixed term $\mathbf{D}^*_{mix}(t)$. In the evaluation of effective dispersion $\mathbf{D}^e(t)$, the contribution of temporal fluctuations alone drops out, and we need to analyze only three terms:

$$\mathbf{D}^e(t) = \mathbf{D} + \mathbf{D}^e_{\delta(Y)}(t) + \mathbf{D}^e_{mix}(t) \tag{35}$$

where, again, the steady state flow contribution $\mathbf{D}^e_{\delta(Y)}(t)$ is known from *Dentz* [2000].

[24] We consider a case of sinusoidal fluctuations of the hydraulic gradient fluctuations $\mathbf{J}$. The component in the x_1-direction remains constant, and that in the x_3-direction zero, whereas the x_2-component oscillates about zero:

$$J_1 = \text{constant} \tag{36}$$

$$J_2 = J_{2,max}\sin\left(\frac{2\pi t}{T} + \varphi\right) \tag{37}$$

$$J_3 = 0 \tag{38}$$

$J_{2,max}$ is the amplitude of the J_2-fluctuations, T is the time for a single cycle, and φ is a random phase-angle differing from realization to realization. Since J_2 is the only random component of $\mathbf{J}$, the temporal covariance matrix $\mathbf{R}_{\mathbf{J}'\mathbf{J}'}(\tau)$ of the mean gradient fluctuations is zero except for the entry $R_{J_2J_2}(\tau)$:

$$R_{J_2J_2}(\tau) = \frac{J^2_{2,max}}{2}\cos\left(\frac{2\pi\tau}{T}\right) \tag{39}$$

[25] In Appendix B, we outline the derivation of closed-form expressions for $D^*_{mix,22}(t)$ and $D^e_{mix,22}(t)$ for a three-dimensional domain with an isotropic, stationary Gaussian covariance function of the log conductivity fluctuations:

$$R_{Y'Y'}(\mathbf{h}) = \sigma_Y^2\exp\left(-\frac{\pi\mathbf{h}^T\mathbf{h}}{4\lambda^2}\right) \tag{40}$$

in which λ is the integral scale. We assume a scalar pore-scale dispersion coefficient D. In the analysis, we use the following dimensionless parameters:

Inverse Peclet number	$\varepsilon = \frac{D}{\langle v_1\rangle\lambda}$
Dimensionless time	$t^* = \frac{t\langle v_1\rangle}{\lambda}$
Relative amplitude of hydraulic gradient fluctuations	$J^* = \frac{J_{2,max}}{J_1}$
Dimensionless frequency of hydraulic gradient fluctuations	$\omega^* = \frac{\lambda}{T\langle v_1\rangle}$

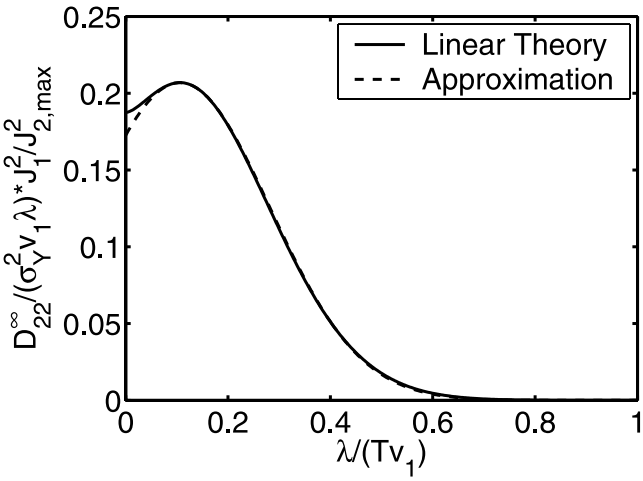

Figure 2. Large-time asymptotic limit of horizontal transverse macrodispersion $D^*_{22}-D^*_{\delta(t),22}$ as function of the frequency of hydraulic gradient fluctuations.

2.4.1. Asymptotic Limit at $t\to\infty$

[26] In the asymptotic limit of $t\to\infty$, the horizontal transverse effective dispersion coefficient $D^e_{22}(t)$ approaches the value of the corresponding macrodispersion coefficient, neglecting the contribution $D^*_{\delta(t),22}(t)$. As derived in Appendix B, the asymptotic value, denoted by D^∞_{22}, is given to first order in ε by:

$$D^\infty_{22} = D + D^\infty_{\delta(Y),22} + D^\infty_{mix,22} \tag{41}$$

with

$$D^\infty_{\delta(Y),22} = \frac{\varepsilon}{3}\sigma_Y^2\lambda\langle v_1\rangle \tag{42}$$

$$\begin{aligned} D^\infty_{mix,22} = {} & \sigma_Y^2\lambda\langle v_1\rangle J^{*2} \\ & \cdot\left(\frac{157}{210}\varepsilon + \frac{1}{2}\left(\exp\left(-4\pi\omega^{*2}\right)\left(\frac{3}{8}+\frac{3}{2}\pi\omega^{*2}\right)\right.\right. \\ & \left.\left. + \frac{1}{4}E_1\left(4\pi\omega^{*2}\right)\left(4\pi\omega^{*2} - 24\pi^2\omega^{*4}\right)\right)\right) \end{aligned} \tag{43}$$

in which $E_1()$ is the exponential integral function which may be approximated by equations 5.1.53 and 5.1.54 of *Abramowitz and Stegun* [1974]. The coefficient for steady state flow, $D^\infty_{\delta(Y),22}$, has already been derived by *Gelhar and Axness* [1983]. $D^\infty_{mix,22}$ is proportional to the squared amplitude of hydraulic gradient fluctuations J^{*2} and depends in a nonlinear way on the frequency ω^*. We have fitted a Gaussian function to $D^\infty_{mix,22}$ leading to the approximation of D^∞_{22}:

$$\begin{aligned} D^\infty_{22} = {} & D + \sigma_Y^2\lambda\langle v_1\rangle \\ & \cdot\left(\frac{\varepsilon}{3} + J^{*2}\left(0.5965\varepsilon + 0.2069\exp\left(-16.15\left(\omega^* - 0.1061\right)^2\right)\right)\right) \end{aligned} \tag{44}$$

[27] Figure 2 shows a plot of D^∞_{22} given by equations (41) and (44) for the strictly advective case, $\varepsilon = 0$, as a

function of the dimensionless frequency ω^*. It is obvious, that the effect of temporal hydraulic gradient fluctuations on the asymptotic transverse dispersion coefficients is dampened at high frequencies. This has already been observed by *Dagan et al.* [1996] and *Zhang and Neuman* [1996] who, however, did not derive closed-form expressions. We observe the maximum enhancement of transverse dispersion at a dimensional frequency ω^* of $\approx 1/9$. The fit by equation (44) is very good for frequencies larger than this value.

2.4.2. Time-Dependent Behavior of Transverse Macrodispersion for the Strictly Advective Case

[28] In the strictly advective case, i.e., $\varepsilon = 0$, the steady state flow contribution $D^*_{\delta(Y),22}(t^*)$ to transverse macrodispersion is:

$$\lim_{\varepsilon\to 0} D^*_{\delta(Y),22}(t^*) = \sigma_Y^2 \lambda \langle v_1 \rangle \left(\operatorname{erf}\left(\frac{t^*\sqrt{\pi}}{2}\right)\left(\frac{1}{\pi t^{*2}} - \frac{6}{\pi^2 t^{*4}}\right) + \frac{6}{\pi^2 t^{*3}} \exp\left(-\frac{\pi t^{*2}}{4}\right)\right) \tag{45}$$

[29] Substituting equation (39) into equation (34) yields the contribution $D^*_{\delta(t),22}(t)$ of temporal fluctuations alone:

$$D^*_{\delta(t),22}(t) = \frac{K_g^2 J_{2,max}^2 T}{\theta^2 4\pi} \sin\left(\frac{2\pi t}{T}\right) \tag{46}$$

which expresses the uncertainty in tagging the plume center because of the randomness in the temporal fluctuations.

[30] Following the approach outlined in Appendix B, the mixed contribution $D^*_{mix,22}(t^*)$ is:

$$\begin{aligned}\lim_{\varepsilon\to 0} D^*_{mix,22}(t^*) = \sigma_Y^2 \lambda \langle v_1 \rangle \frac{J^{*2}}{4} \Bigg(& \left(\operatorname{erf}\left(\frac{\sqrt{\pi}}{2} t^* - 2\sqrt{\pi} i\omega^*\right) + \operatorname{erf}\left(\frac{\sqrt{\pi}}{2} t^* + 2\sqrt{\pi} i\omega^*\right)\right)\left(\left(\frac{3}{8} + \frac{3}{2}\pi\omega^{*2}\right)\right. \\ & \left. \cdot \exp\left(-4\pi\omega^{*2}\right) + E_1\left(4\pi\omega^{*2}\right)\left(\pi\omega^{*2} - 6\pi^2\omega^{*4}\right)\right) \\ & + \frac{4}{\sqrt{\pi}} \exp\left(-\frac{\pi}{4} t^{*2} + 4\pi\omega^{*2}\right) \\ & \cdot \left(\cos(2\pi\omega^* t^*)\frac{\sqrt{\pi}}{2} t^* - \sin(2\pi\omega^* t^*) 2\sqrt{\pi}\omega^*\right) \\ & \cdot \left(\left(\frac{1}{16} + \frac{3}{4}\pi\omega^{*2}\right)\exp\left(-4\pi\omega^{*2}\right) + E_1\left(4\pi\omega^{*2}\right)\right. \\ & \left. \cdot \left(\frac{1}{8} - \pi\omega^{*2} - 3\pi^2\omega^{*4}\right)\right)\Bigg)\end{aligned} \tag{47}$$

[31] Equation (47) contains the sum of two error functions with complex arguments. Since the arguments are the complex conjugates of each other, the resulting expression is real. In the numerical evaluation, we have used equation 7.1.29 of *Abramowitz and Stegun* [1974] as approximation of the error function with complex arguments.

[32] Figure 3 shows all contributions to the horizontal transverse macrodispersion coefficient $D^*_{22}(t)$ in the strictly advective case for the following parameters:

$$\begin{array}{llll} \sigma_Y^2 = 1, & \lambda = 1m, & K_g = 10^{-4} m/s, & \theta = 0.25, \\ J_1 = 0.01, & J_{2,\max} = J_1/2, & T = 10d & \end{array}$$

[33] The solid line marks the contribution $D^*_{\delta(Y),22}(t)$ by the spatial variability of log conductivity alone as calculated by equation (45). This is identical to $D^*_{22}(t)$ under steady flow conditions. It shows the well-known maximum at early times reflecting uncertainty in the plume meandering. Graphically speaking, due to random spatial variability, we do not know whether the meandering of a point-related plume starts with a left or a right turn. The related uncertainty in the transverse plume position does no more increase at late times.

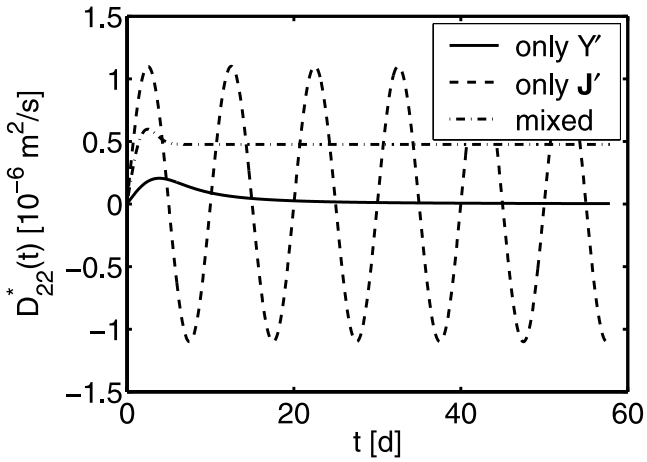

Figure 3. Contributions to the horizontal transverse macrodispersion coefficient $D^*_{22}(t)$ for random temporal fluctuations.

[34] The dashed line in Figure 3 is the contribution $D^*_{\delta(t),22}(t)$ from temporal variability of the mean hydraulic gradient alone, according to equation (34). For the case of sinusoidal fluctuations, it exhibits negative values because the uncertainty in tagging the center of the plume due to the gradient-fluctuations becomes zero for t being an integer multiple of T. In the approach of *Rehfeldt and Gelhar* [1992], the contributions $D^*_{\delta(Y),22}(t)$ and $D^*_{\delta(t),22}(t)$ are summed up.

[35] The dash-dotted line in Figure 3 marks the mixed term $D^*_{mix,22}(t)$ that has been omitted by *Rehfeldt and Gelhar* [1992]. For the chosen parameters, it has a maximum that coincides with the first maximum of $D^*_{\delta(t),22}(t)$, and levels out to a constant value at later times. For higher values of the dimensionless frequency ω^*, $D^*_{mix,22}(t)$ may show more extrema corresponding to the oscillations of $D^*_{\delta(t),22}(t)$.

[36] For the chosen parameters, all three contributions are of similar importance at early times. At late times, $D^*_{\delta(Y),22}(t)$ vanishes. With a smaller variance σ_Y^2 of the log conductivity, the uncertainty in the mean hydraulic gradient would have dominated the uncertainty in tagging the lateral position of the plume center. By changing from random to deterministic temporal fluctuations, however, the contribution $D^*_{\delta(t)22}(t)$ would disappear. By contrast, the mixed term $D^*_{mix,22}(t)$ does also occur for the case of deterministic fluctuations. Particularly in the large-time limit, $D^*_{mix,22}(t)$ expresses the mean enhancement of horizontal transverse macrodispersion due to changes in the hydraulic gradient for both random and deterministic fluctuations.

2.4.3. Approximation of Time-Dependent Behavior of Transverse Effective Dispersion

[37] While the transverse-macrodispersion contributions $D^*_{\delta(Y),22}(t)$ and $D^*_{mix,22}(t)$ show distinct maxima at early

times, this is not the case for effective dispersion. Macrodispersion contains the uncertainty in the trajectory of the plume center. Particularly at early times, when $D^*_{\delta(Y),22}(t)$ and $D^*_{mix,22}(t)$ have their maxima, this uncertainty dominates $D^*_{22}(t)$. Effective dispersion, by contrast, expresses the lateral expansion of the point-related plume itself and is not influenced by the uncertainty in the starting angle between the true trajectory of the plume center and its expected value.

[38] As outlined in Appendix B, we can derive an approximation for the time-dependent transverse effective dispersion coefficient $D^e_{22}(t)$:

$$D^e_{22}(t) \approx D + \frac{2\pi\varepsilon t^*}{1+2\pi\varepsilon t^*} D^{\infty}_{\delta(Y),22} + \left(1 - \frac{\exp\left(-2\pi^2\omega^{*2}\varepsilon t^*\right)}{1+2\pi\varepsilon t^*}\right) D^{\infty}_{mix,22} \tag{48}$$

It may be noteworthy that the impact of pore-scale dispersion in the exponential term comes from longitudinal local dispersion. This is different to steady state flows, where longitudinal pore-scale dispersion does not influence effective transverse dispersion. In transient flow, the direction of the streamlines changes over time, so that a plume that spreads out into the longitudinal direction becomes also wider, although the effect is not very pronounced.

[39] Equation (48) is an algebraic expression that, with the exception of the exponential term, is formally equivalent to a Michaelis-Menten term. For the parameters given above and a realistic value of pore-scale transverse dispersion on the order of ten times the molecular diffusion coefficient, the local-dispersive half-time $\lambda^2/(2\pi D)$ is $\approx 200d$. The exponential expression makes effective dispersion catch up slightly faster. One should keep in mind, however, that equation (48) holds for an isotropic spatial covariance function. In an anisotropic medium, we have two dispersive time-scales, one proportional to the large horizontal integral scale, and the other to the small vertical one [*Dentz et al.*, 2000a]. Here pore-scale dispersion in the vertical direction dominates the time-dependent behavior of effective dispersion.

2.5. Semianalytical Evaluation by Discrete Fourier Transformation

[40] In addition to the closed-form expressions holding only for an isotropic Gaussian covariance model of the log conductivity fluctuations, we evaluate the two dispersion tensors by numerical operations in a discretized spectral domain and subsequent discrete back-transformation into the spatial domain. The numerical evaluation of equations (31) and (32) allows a higher flexibility in choosing the covariance model $R_{Y'Y'}(\mathbf{h})$. As discussed in Appendix C, we apply fast Fourier transformation (FFT) techniques. FFT applies to Fourier series rather than integrals. This is equivalent to assuming a periodic rather than a stationary log conductivity field [*Dykaar and Kitanidis*, 1992]. The log conductivity values are identical at integer multiples of the unit length L_i in each direction x_i:

$$Y(\mathbf{x} + n\mathbf{e}_i L_i) = Y(\mathbf{x}) \tag{49}$$

in which $\mathbf{e}_i$ is the unit length vector in direction i. The fluctuations within a single unit cell are characterized by the periodic covariance function $R_{Y'Y'}(\mathbf{h})$ with the following property:

$$\langle Y'(\mathbf{x})Y'(\mathbf{x}+\mathbf{h})\rangle = R_{Y'Y'}(\mathbf{h}) = R_{Y'Y'}(n\mathbf{e}_i L_i - \mathbf{h}) \tag{50}$$

[41] The perfect correlation at integer multiples of the unit lengths lead to artifacts in the evaluation of dispersion terms. While in stationary media the dispersion coefficients approach an asymptotic value in a single smooth step, periodic media show multiple steps associated with the mean displacement being about an integer multiple of the unit length. By choosing large unit lengths and restricting the considered travel time so that the mean displacement is considerably smaller than the unit length, the macrodispersion coefficients for periodic media are essentially identical to those for the corresponding stationary media.

2.6. Deterministic Temporal Fluctuations

[42] In this section, we consider the case of deterministic fluctuations of the mean hydraulic gradient, i.e., $\langle \nabla\phi(\mathbf{x},t)\rangle = -\mathbf{J}(t)\forall\mathbf{x}$. This case was considered in the analysis of macrodispersion for strictly advective transport by *Zhang and Neuman* [1996] and *Dagan et al.* [1996], and for advective-dispersive transport by *Wood and Kavvas* [1999]. The cross-spectrum of specific discharge fluctuations $\mathbf{q}'$ at times t' and t'' is given by:

$$\mathbf{S}_{\mathbf{q}'(t')\mathbf{q}'^T(t'')}(\mathbf{s}) = K_g^2 \left(\mathbf{J}(t') - \frac{\mathbf{s}\mathbf{s}^T\mathbf{J}(t')}{\mathbf{s}^T\mathbf{s}}\right)\left(\mathbf{J}(t'') - \frac{\mathbf{s}\mathbf{s}^T\mathbf{J}(t'')}{\mathbf{s}^T\mathbf{s}}\right)^T S_{Y'Y'}(\mathbf{s}) \tag{51}$$

Without repeating the details of the derivation, the resulting macrodispersion and effective dispersion tensors, $\mathbf{D}^*(t)$ and $\mathbf{D}^e(t)$, are now:

$$\mathbf{D}^*(t) = \mathbf{D} + \int_{\infty}\int_{0}^{t} \mathrm{sym}\left(\mathbf{S}_{\mathbf{v}'(t')\mathbf{v}(t)}(\mathbf{s})\right) \cdot \exp\left((-4\pi^2\mathbf{s}^T\mathbf{D}\mathbf{s}(t-t') + 2\pi i\mathbf{s}^T(\langle\mathbf{X}(t)\rangle - \langle\mathbf{X}(t')\rangle))\right)dt'd\mathbf{s} \tag{52}$$

$$\mathbf{D}^e(t) = \mathbf{D}^*(t) - \int_{\infty}\int_{0}^{t} \mathrm{sym}\left(\mathbf{S}_{\mathbf{v}'(t')\mathbf{v}'(t)}(\mathbf{s})\right) \cdot \exp\left(-4\pi^2\mathbf{s}^T\mathbf{D}\mathbf{s}(t'+t) + 2\pi i\mathbf{s}^T(\langle\mathbf{X}(t)\rangle - \langle\mathbf{X}(t')\rangle)\right)dt'd\mathbf{s} \tag{53}$$

in which $\langle\mathbf{x}(t)\rangle = \int_0^t\langle\mathbf{v}(\tau)\rangle\, d\tau$ is the mean trajectory of the plume center, $\mathbf{S}_{\mathbf{v}'(t')\mathbf{v}(t)}(\mathbf{s}) = \mathbf{S}_{\mathbf{q}'(t')\mathbf{q}'(t)}(\mathbf{s})/\theta^2$ is the cross-spectrum of seepage-velocity fluctuations at times t' and t, and sym() is the symmetry operator: $\mathrm{sym}(\mathbf{A}) = \frac{1}{2}(\mathbf{A}+\mathbf{A}^T)$. For the case of zero local dispersion, i.e., $\mathbf{D} = \mathbf{0}$, equation (52) simplifies to the solution of *Zhang and Neuman* [1996]:

$$\mathbf{D}^*_{\mathbf{D}=\mathbf{0}}(t) = \int_{\infty}\int_{0}^{t} \mathrm{sym}\left(\mathbf{S}_{\mathbf{v}'(t')\mathbf{v}(t)}(\mathbf{s})\right) \exp\left(2\pi i\mathbf{s}^T(\langle\mathbf{X}(t)\rangle - \langle\mathbf{X}(t')\rangle)\right)dt'd\mathbf{s} = \int_0^t \mathrm{sym}\left(\mathbf{R}_{\mathbf{v}'(t')\mathbf{v}(t)}(\langle\mathbf{X}(t)\rangle - \langle\mathbf{X}(t')\rangle)\right)dt' \tag{54}$$

$$\mathbf{D}^e_{\mathbf{D}=\mathbf{0}}(t) = \mathbf{0} \tag{55}$$

[43] Evaluating the expressions for deterministic temporal fluctuations, equations (52) and (53), is computationally more demanding than the corresponding expressions for random fluctuations, equations (31) and (32). For each time t, the temporal integrals in equations (52) and (53) must be fully re-evaluated, regardless of previous evaluations at smaller t-values. This is so because the time t itself appears in the nonlinear terms $\mathbf{S}_{\mathbf{v}'(t')\mathbf{v}'(t)}(\mathbf{s})$ and $\langle \mathbf{X}(t) \rangle$ within the temporal integral. By contrast, the temporal integrals in equations (31) and (32) contain expressions that are translationally invariant in time, namely $\mathbf{S}_{\mathbf{v}'\mathbf{v}'^T}(\mathbf{s}, \tau)$ and $\langle \mathbf{v} \rangle \tau$. Therefore previous evaluations at smaller t-values can directly be utilized. If we consider a numerical time-integration scheme over 1000 time steps, equations (31) and (32) require 1000 evaluations of the term within the time-integral and equations (52) and (53) 500,000. Also, the derivation of the closed-form expression requires translational invariance in time. It is therefore computationally advantageous to use the expressions for random rather than deterministic temporal fluctuations.

[44] The macrodispersion tensor $\mathbf{D}^*(t)$ given in equation (52) differs qualitatively from that in equation (31), because it is not affected by uncertainty in the temporal fluctuations. To make the two macrodispersion tensors more comparable, we eliminate the effect of temporal uncertainty alone from $\mathbf{D}^*(t)$ in equation (31) by neglecting the term $\mathbf{D}^*_{\delta(t)}(t)$ given by equation (34).

3. Comparative Particle-Tracking Random-Walk Simulation

[45] For given geostatistical parameters, we generate periodic random fields by a spectral approach similar to that of *Dykaar and Kitanidis* [1992]. With the time-dependent mean head gradient $\mathbf{J}(t)$, the hydraulic heads ϕ in the infinite, periodic domain exhibit a linear trend with periodic fluctuations. Except for a constant, the field is fully described by the hydraulic-head distribution within a single unit cell with periodic boundary conditions [*Kitanidis*, 1992; *Dykaar and Kitanidis*, 1992]:

$$\phi(L_1, x_2, x_3, t) = \phi(0, x_2, x_3, t) - J_1(t) L_1 \tag{56}$$

$$\phi(x_1, L_2, x_3, t) = \phi(x_1, 0, x_3, t) - J_2(t) L_2 \tag{57}$$

$$\phi(x_1, x_2, L_3, t) = \phi(x_1, x_2, 0, t) - J_3(t) L_3 \tag{58}$$

Because the fields of log hydraulic conductivity $Y(\mathbf{x})$ and the hydraulic head fluctuations $\phi'(\mathbf{x})$ are periodic, the fields of specific discharge and seepage velocity $\mathbf{v}$ are also periodic and thus fully described by the distribution within a single cell. In our simulations, the flow field is evaluated by a standard cell-centered finite volume formulation for each realization, accounting for the periodic boundary conditions, Equations (56–58). The linear system of equations is solved by a conjugate gradient solver with algebraic multigrid preconditioning [*Ruge and Stüben*, 1987].

[46] Transport is solved by the particle-tracking random-walk method using the semianalytical approach of *Pollock* [1988] for the advective displacement. We replace the expected-value operator by the average over many particle pairs introduced at different points of a single flow field. The particle pairs are introduced at the centers of all finite volume cells and tracked through the periodic domain. A particle leaving a unit cell at a boundary enters an adjacent unit cell with identical flow field. That is, we can reintroduce the particle at the opposite side of the unit cell and add/subtract the corresponding length L_i to/from the particle's position within the unit cell to gain its global position. The one-particle variance of displacement $\langle \mathbf{X}'\mathbf{X}'^T \rangle (t)$ at time t is evaluated by:

$$\begin{aligned}\langle \mathbf{X}'\mathbf{X}'^T \rangle(t) = {} & \frac{1}{2n_c}\left(\sum_{k=1}^{n_c} \mathbf{X}_1(k,t)\mathbf{X}_1^T(k,t) + \mathbf{X}_2(k,t)\mathbf{X}_2^T(k,t)\right) \\ & - \frac{1}{4n_c^2}\left(\sum_{k=1}^{n_c} \mathbf{X}_1(k,t) + \mathbf{X}_2(k,t)\right) \\ & \cdot \left(\sum_{k=1}^{n_c} \mathbf{X}_1^T(k,t) + \mathbf{X}_2^T(k,t)\right)\end{aligned} \tag{59}$$

in which n_c is the number of Finite Volume cells, $\mathbf{X}_1(k, t)$ is the displacement at time t of particle 1 starting at time zero in the center of cell k, and $\mathbf{X}_2(k, t)$ is the same quantity for particle 2. The displacement is the actual position of the particle at time t minus the coordinates of the starting point. The two-particle semivariogram of displacement $\mathbf{\Gamma}_{\mathbf{x}\mathbf{x}'}(t)$ is given by:

$$\begin{aligned}\mathbf{\Gamma}_{\mathbf{X}\mathbf{X}^T}(t) &\equiv \langle \mathbf{X}'\mathbf{X}'^T \rangle(t) - \langle \mathbf{X}_1'\mathbf{X}_2'^T \rangle(t) \\ &= \frac{1}{2n_c}\left(\sum_{k=1}^{n_c} (\mathbf{X}_1(j,k,t) - \mathbf{X}_2(j,k,t)) \cdot (\mathbf{X}_1^T(j,k,t) - \mathbf{X}_2^T(j,k,t)\right)\end{aligned} \tag{60}$$

The one-particle variance of displacement $\langle \mathbf{X}'\mathbf{X}'^T \rangle$ (t) and the two-particle semivariogram of displacement $\mathbf{\Gamma}_{\mathbf{x}\mathbf{x}'}(t)$ are evaluated at discrete times. Subsequently, the macrodispersion and effective dispersion tensors are calculated by numerical differentiation with respect to time:

$$\mathbf{D}^*(t) = \frac{1}{2}\frac{\langle \mathbf{X}'\mathbf{X}'^T \rangle(t + \Delta t) - \langle \mathbf{X}'\mathbf{X}'^T \rangle(t)}{\Delta t} \tag{61}$$

$$\mathbf{D}^e(t, \mathbf{0}) = \frac{1}{2}\frac{\mathbf{\Gamma}_{\mathbf{X}\mathbf{X}^T}(t + \Delta t) - \mathbf{\Gamma}_{\mathbf{X}\mathbf{X}^T}(t)}{\Delta t} \tag{62}$$

In the numerical simulations, the temporal fluctuations of the mean hydraulic gradient $\mathbf{J}(t)$ are deterministic. As discussed above, we assume sinusoidal fluctuations of the mean hydraulic gradient $\mathbf{J}(t)$. Within this model, random fluctuations of the head gradient would refer to a random phase angle. The mean behavior over all phase angles would be determined by averaging the results for deterministic fluctuations over all phase angle. We simplify the averaging by considering only two phase-angles: 0 and $\pi/2$. We apply the particle-tracking random walk method to the flow fields resulting from the two phase angles, calculate the macrodispersion and effective dispersion tensors, $\mathbf{D}^*(t)$

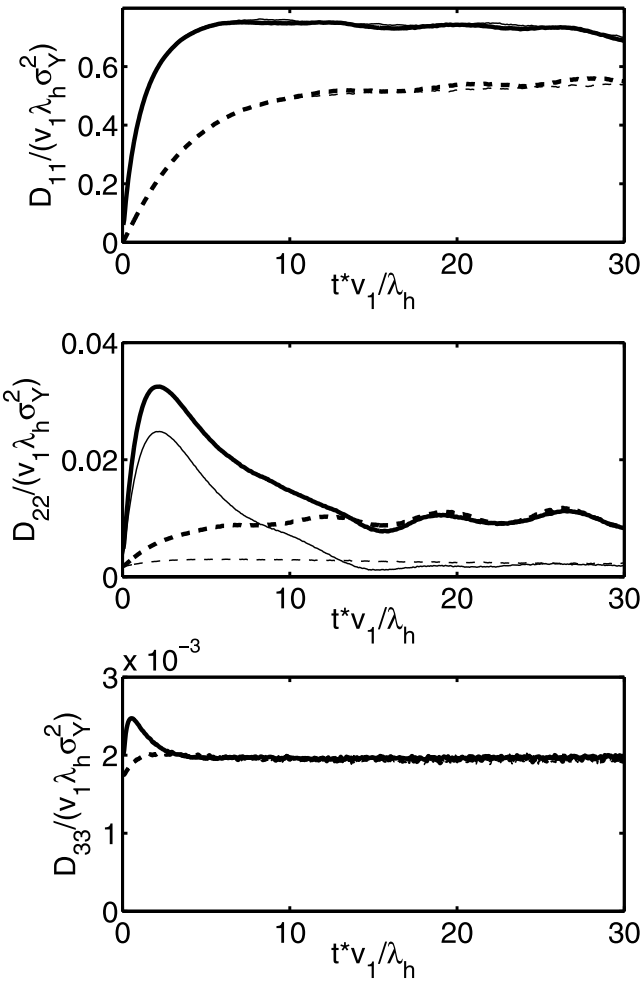

Figure 4. Components of the dispersion tensors for Borden-like conditions evaluated by particle-tracking random-walk simulations. Solid lines, macrodispersion ($\mathbf{D}^*(t)-\mathbf{D}^*_{\delta(t)}$); dashed lines, effective dispersion; thin lines, steady state flow; thick lines, transient flow.

and $\mathbf{D}^e(t, \mathbf{0})$, according to equations (61) and (62) for both phase angles and take the average.

4. Application to a Borden-Like Test Case

[47] In the following, we evaluate the macrodispersion and effective dispersion tensor for a three-dimensional random periodic domain by the semianalytical approach using discrete Fourier transformation. As in section 2.4, we consider sinusoidal fluctuations of the mean hydraulic gradient with a random phase angle, Equations (36–39). For the spatial log conductivity fluctuations, we assume the anisotropic exponential covariance model:

$$R_{Y'Y'}(\mathbf{h}) = \sigma_Y^2 \exp\left(-\sqrt{\frac{h_1^2+h_2^2}{\lambda_h^2}+\frac{h_3^2}{\lambda_v^2}}\right) \tag{63}$$

in which σ_Y^2 is the log conductivity variance, and λ_h and λ_v are the horizontal and vertical correlation lengths, respectively.

[48] We compare results from linear theory to those from particle-tracking random-walk simulations for a fictitious aquifer with coefficients comparable to the Borden site. As listed in Table 1, the parameters were taken from *Woodbury and Sudicky* [1991] and *Rajaram and Gelhar* [1993] regarding the log conductivity field and from *Bellin et al.* [1996] regarding the transient behavior of flow. The fluctuations in the direction of flow are limited to ±10.4°.

4.1. Comparison Between Linear Theory and Particle-Tracking Random-Walk Simulations

[49] Figure 4 shows a comparison of the diagonal components of the dispersion tensors evaluated by particle-tracking random-walk simulations for steady state and transient flow. Time is normalized by the mean advective travel time for a single horizontal correlation length $\lambda_h/\bar{v}_1$, and the dispersion coefficients are normalized by $\bar{v}_1\lambda_h\sigma_Y^2$ in which $\bar{v}_1$ is the observed mean velocity. The results for steady state flow are shown as thin lines and those for transient flow as bold lines. Obviously, the transient and steady state results are almost identical for the mean longitudinal and the vertical directions. In the vertical direction, heterogeneity hardly increases dispersion at all. In

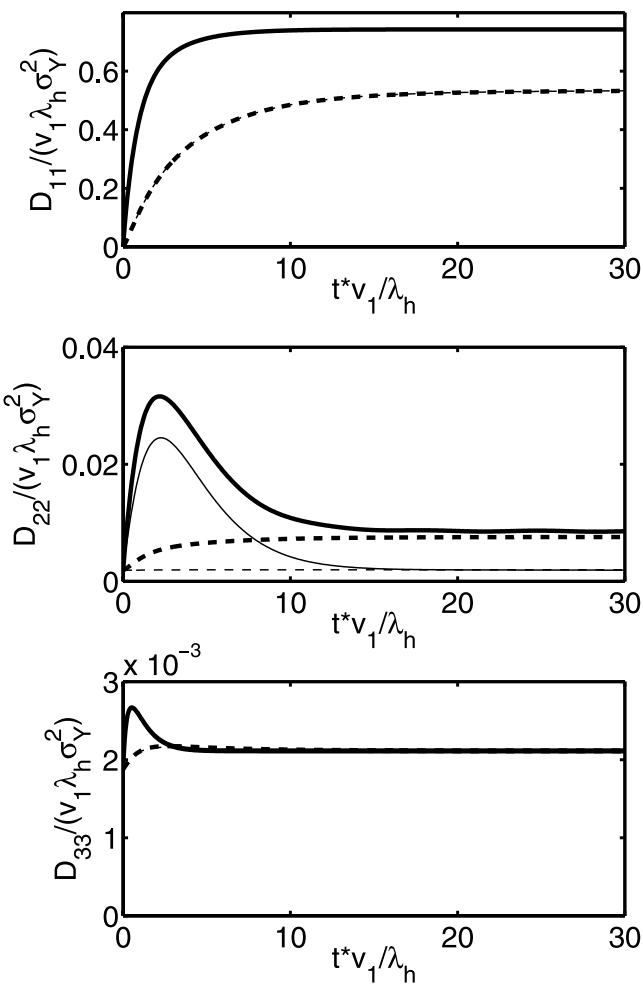

Figure 5. First-order prediction of dispersion tensors components for Borden-like conditions. Solid lines, macrodispersion ($\mathbf{D}^*(t)-\mathbf{D}^*_{\delta(t)}$); dashed lines, effective dispersion; thin lines, steady state flow; thick lines, transient flow.

Table 1. Parameters Used for the Simulation of a Borden-Like Aquifer

Parameter	Value
Log Conductivity Field[a]	
K_{g_2}	7.17×10^{-5} m/s
σ_Y^2	0.24
λ_v	0.21 m
λ_h	5.1 m
Type	exponential
Mean Hydraulic Gradient[b]	
J_1	4×10^{-3}
T	450 d = 3.888×10^7 s
$J_{2,max}/J_1$	0.184
Discretization	
L	250 m × 60 m × 2 m
Δ**x**	0.5 m × 0.5 m × 0.025 m
Δt	$2.65 \times 10^5 s$ = 3d 1h 44′
Transport Properties[c]	
θ	0.33
D	2×10^{-9} m^2/s

[a] *Woodbury and Sudicky* [1991] and Rajaram and *Gelhar* [1993].
[b] *Bellin et al.* [1996].
[c] *Woodbury and Sudicky* [1991].

the horizontal transverse direction x_2, the transient simulations show a higher maximum transverse macrodispersivity than the steady state simulations. More importantly, both macrodispersion and effective dispersion in the x_2-direction approach an asymptotic value that is about five times higher than in the steady-state flow case.

[50] Figure 5 shows the predicted values for the dispersion tensor components applying linear theory. Here, to be consistent in the order of approximation, the velocity for normalization is $\langle v_1 \rangle^{(1)} = K_g J_1/\theta$. As observed in the particle-tracking random-walk simulations, the transient flow behavior does hardly affect the dispersion coefficients in the x_1- and x_3-directions. The results for the x_2-direction agree qualitatively very well with the particle simulations. Figure 6 shows a direct comparison between the numerical and semianalytical results for D_{22}^* and D_{22}^e under transient flow conditions. The particle results show fluctuations about the mean that are presumably caused by the limited size of the computational domain. The peaks of transverse macrodispersivity are predicted very well by linear theory, whereas the particle results appear to approach a slightly higher asymptotic value than predicted by linear theory. Also, the particle results indicate that the effective horizontal transverse dispersivity catches completely up with the corresponding macrodispersivity after passing about 15 integral scales, whereas linear theory predicts a small but distinct difference between both types of dispersivity over a longer time period. These minor differences might be caused by higher-order effects. A particular reason might be that the plume expands faster in the transverse direction under transient than under steady state flow conditions.

4.2. Comparison Between Random and Deterministic Temporal Fluctuations

[51] Figure 7 shows a comparison of the horizontal transverse dispersion coefficients between predictions from linear theory for deterministic and random temporal oscillations of the mean hydraulic gradient $\mathbf{J}(t)$. As in the particle-tracking random-walk simulations, the deterministic oscillations are for a phase angle φ of 0 and $\pi/2$. The results from particle tracking are indicated in Figure 7 by symbols. Because of the high computational effort, the semianalytical calculations for deterministic oscillations have been performed for a much shorter time period than those for random oscillations. It is obvious that for the given set of parameters both $D_{22}^*(t)$ and $D_{22}^e(t)$ for the deterministic oscillations, according to equations (52) and (53), fluctuate about the estimate $D_{22}^*(t) - D_{22,\delta(t)}^*(t)$ and $D_{22}^e(t)$ for random oscillations according to equations (31) and (32). The agreement with the particle-tracking random-walk simulations is fairly good.

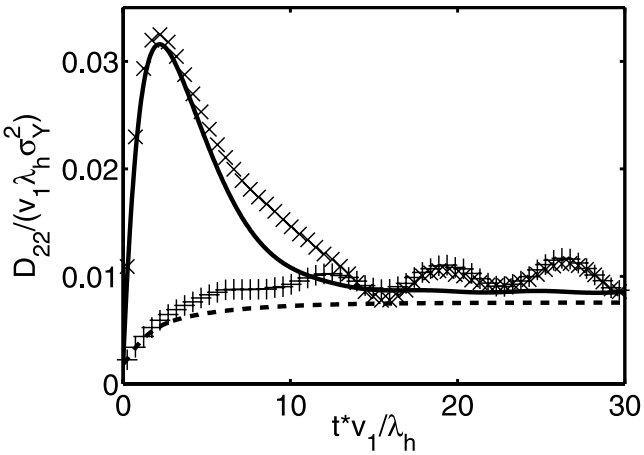

Figure 6. Horizontal transverse dispersion under transient flow conditions. Comparison between results from particle-tracking random-walk (symbols) and first-order stochastic theory for horizontal transverse dispersivity (lines). Solid lines and crosses, macrodispersion ($D_{22}^*(t) - D_{22,\delta(t)}^*$); dashed lines and pluses, effective dispersion, D_{22}^e.

[52] The deterministic calculations show distinct peaks in both types of transverse horizontal dispersion which coincide with the times at which the absolute transverse

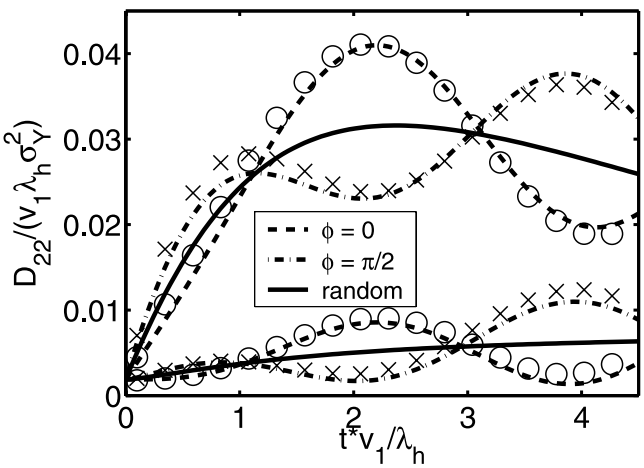

Figure 7. Horizontal transverse dispersion coefficients. Comparison between results of linear theory for deterministic and random fluctuations of the mean hydraulic gradient. Lines, linear theory; symbols, particle-tracking/random-walk simulations.

gradient component is the highest. These peaks, of course, cannot be captured with an unknown phase angle. The good agreement with the average coefficients related to the two phase angles, however, indicates that following the space-time mean trajectory in the approach of random gradient oscillations does not introduce severe bias as long as the fluctuations of the trajectory are small. With the parameters used in this study, the mean trajectory oscillated $\pm 0.2\lambda_h$ about its temporal average. Trajectory oscillations of significantly more than one horizontal correlation length may lead to stronger differences between results of deterministic and random temporal gradient fluctuations.

5. Conclusions

[53] Temporal fluctuations in the orientation of the mean hydraulic gradient enhances long-time transverse dispersion, but not to the extent predicted by the classical model of uniform dispersion in homogeneous media [*Kinzelbach and Ackerer*, 1986; *Goode and Konikow*, 1990]. This has already been shown for macrodispersion by *Dagan et al.* [1996] and *Zhang and Neuman* [1996]. Our findings are in agreement to those of the latter studies, extending the results to effective dispersion for a point-like injection. Taking effective dispersion as a measure of actual dispersive mixing, the present results indicate that transverse dispersive mixing depends strongly on transient flow behavior. This might be important in assessing natural attenuation of a quasi-steady state plume of a contaminant introduced continuously into an aquifer.

[54] We have derived a first-order spectral solution for macrodispersion and effective dispersion in stationary heterogeneous media with random fluctuations of the mean head gradient. Comparative particle-tracking random-walk simulations show a good agreement to the analytical results for small temporal fluctuations of the mean head gradient as observed at the Borden test site. We have also performed particle simulations in which the direction of flow fluctuates by ±45°. The results of the latter study, not shown here, indicate that effective dispersion approaches the value of macrodispersion faster under transient than under steady state flow conditions. This behavior cannot be predicted by linear theory. Against this background, it might be worthwhile to assess the higher-order terms appearing in the derivation of effective dispersion in more detail when considering cases of strong temporal fluctuations. Such derivations, however, are beyond the scope of the present study.

[55] While we strongly believe that an accurate estimation of transverse mixing rates is essential in the assessment of natural attenuation, it remains challenging to solve the problem solely by analytical means. The present study demonstrates that the temporal evolution of transverse effective dispersion can be predicted sufficiently well for small fluctuations of transverse flow, however, the following limitations and practical difficulties remain: (1) Effective dispersion coefficients, particularly at early times, depend strongly on pore-scale transverse dispersion coefficients which are difficult to determine [*Klenk and Grathwohl*, 2002]. (2) The analytical results for effective dispersion derived so far assume stationary velocity fields which might be unrealistic in many field situations. Recent advances achieved for macrodispersion in nonstationary media assuming strictly advective transport [*Indelman and Rubin*, 1996; *Zhang*, 1998; *Zhang et al.*, 2000] cannot be transferred to effective dispersion which is strongly affected by pore-scale dispersion. (3) Effective dispersion coefficients derived from stochastic theory are expected values and hold for single realizations only when the ergodicity assumption is valid. Since the mixing of a plume with ambient water occurs within a narrow stripe along the dividing surface, the supporting volume is presumably too small to justify such an assumption. Therefore the mixing rates occurring in the decisive fringes of a plume might differ considerably from their predicted values. Against this background, it might be advisable to perform Monte-Carlo simulations of particle transport to come up with estimates of effective mixing rates and their uncertainty. Such simulations do not require stationarity of the flow field and can be conditioned on all data available.

Appendix A: Spatial Moments

[56] The zeroth spatial moment $m_0(c(\mathbf{x}, t)) = \int_\infty c(\mathbf{x}, t)d\mathbf{x}$ is the total mass of the solute which remains constant at all times in all realizations. Because of the initial condition, equation (22), $m_0(c(\mathbf{x}, t))$ is unity. For a nonunity mass, the higher spatial moments given below are the moments normalized by the solute mass.

[57] The vector of first spatial moments $\mathbf{m}_\mathbf{x}(c(\mathbf{x}, t))$ of the concentration is obtained by:

$$\mathbf{m}_\mathbf{x}(c(\mathbf{x},t)) \equiv \int_\infty \mathbf{x}c(\mathbf{x},t)d\mathbf{x} = \frac{i}{2\pi}\nabla_\mathbf{s}\tilde{c}(\mathbf{s},t)|_{\mathbf{s}=\mathbf{0}} = \frac{i}{2\pi}\nabla_\mathbf{s}\tilde{c}_0(\mathbf{s},t)|_{\mathbf{s}=\mathbf{0}} + \int_\infty \int_0^t \int_\infty \tilde{\mathbf{v}}'(\mathbf{s}',\omega)\exp(2\pi i\omega t'))d\omega\tilde{c}_0(-\mathbf{s}',t')dt'd\mathbf{s}' \tag{A1}$$

in which $\nabla_\mathbf{s}$ is the gradient with respect to the $\mathbf{s}$-coordinates in the spectral domain.

[58] The first spatial moments $\mathbf{m}_\mathbf{x}(\langle c(\mathbf{x}, t)\rangle)$ of the expected concentration equal the expected values of the first moments $\langle \mathbf{m}_\mathbf{x}(c(\mathbf{x}, t))\rangle$:

$$\mathbf{m}_\mathbf{x}(\langle c(\mathbf{x},t)\rangle) = \langle \mathbf{m}_\mathbf{x}(c(\mathbf{x},t))\rangle = \frac{i}{2\pi}\nabla_\mathbf{s}\langle\tilde{c}(\mathbf{s},t)\rangle|_{\mathbf{s}=\mathbf{0}} = \frac{i}{2\pi}\nabla_\mathbf{s}\tilde{c}_0(\mathbf{s},t)|_{\mathbf{s}=\mathbf{0}} = \langle\mathbf{v}\rangle t \tag{A2}$$

Subtracting equation (A2) from equation (A1), multiplying the expression with its transpose and taking the expected value as well as the derivative with respect to time yields the rate of change of the covariance matrix of first-moment deviations $\langle \mathbf{m}'_\mathbf{x}(c(\mathbf{x}, t))\mathbf{m}'^T_\mathbf{x}(c(\mathbf{x}, t))\rangle$:

$$\frac{\partial\langle \mathbf{m}'_\mathbf{x}(c(\mathbf{x},t))\mathbf{m}'^T_\mathbf{x}(c(\mathbf{x},t))\rangle}{\partial t} = 2\int_\infty \int_0^t \mathcal{S}_{\mathbf{v}'\mathbf{v}'^T}(\mathbf{s},t-t')\tilde{c}_0(-\mathbf{s},t) \cdot \tilde{c}_0(\mathbf{s},t')dt'd\mathbf{s} \tag{A3}$$

which will be needed below.

[59] The matrix of second noncentral spatial moments $\mathbf{M}_{\mathbf{x}\mathbf{x}^T}(c(\mathbf{x}, t))$ is defined as:

$$\mathbf{M}_{\mathbf{x}\mathbf{x}^T}(c(\mathbf{x},t)) \equiv \int_{\infty} \mathbf{x}\mathbf{x}^T c(\mathbf{x},t) d\mathbf{x} = -\frac{1}{4\pi^2} \boldsymbol{\nabla}_{\mathbf{s}} \boldsymbol{\nabla}_{\mathbf{s}}^T \tilde{c}(\mathbf{s},t)\big|_{\mathbf{s}=\mathbf{0}} \quad \text{(A4)}$$

[60] As in the case of the first moments, the second noncentral moments of the expected concentration $\mathbf{M}_{\mathbf{x}\mathbf{x}^T}(\langle c(\mathbf{x}, t)\rangle)$ equal the expected value of the second noncentral moments $\langle \mathbf{M}_{\mathbf{x}\mathbf{x}^T}(c(\mathbf{x}, t))\rangle$:

$$\frac{\partial \mathbf{M}_{\mathbf{x}\mathbf{x}^T}(\langle c(\mathbf{x},t)\rangle)}{\partial t} = \frac{\partial \langle \mathbf{M}_{\mathbf{x}\mathbf{x}^T}(c(\mathbf{x},t))\rangle}{\partial t} = -\frac{1}{4\pi^2}\frac{\partial}{\partial t}\left(\boldsymbol{\nabla}_{\mathbf{s}} \boldsymbol{\nabla}_{\mathbf{s}}^T \tilde{c}_0(\mathbf{s},t)\big|_{\mathbf{s}=\mathbf{0}}\right) + 2\int_{\infty}\int_{0}^{t} \frac{\tilde{c}_0(-\mathbf{s},t)}{\tilde{c}_0(-\mathbf{s},t')} \mathcal{S}_{\mathbf{v}'\mathbf{v}'^T}(\mathbf{s}, t-t') dt' d\mathbf{s} \quad \text{(A5)}$$

[61] The second central moment $\mathbf{M}^c_{\mathbf{x}\mathbf{x}^T}(c(\mathbf{x}, t))$ of the concentration is defined as:

$$\mathbf{M}^c_{\mathbf{x}\mathbf{x}^T}(c(\mathbf{x},t)) \equiv \mathbf{M}_{\mathbf{x}\mathbf{x}^T}(c(\mathbf{x},t)) - \mathbf{m}_{\mathbf{x}}(c(\mathbf{x},t))\mathbf{m}_{\mathbf{x}}^T(c(\mathbf{x},t)) \quad \text{(A6)}$$

[62] In contrast to the noncentral moments, the expected value of the second central moment differs from the second central moment of the expected concentration by the covariance of the first-moment deviations, with the rate of change given in equation (A3). Taking the temporal derivative of equation (A6) and considering the expected values of (1) the concentration and (2) the second central moment, respectively, yields:

$$\frac{\partial \mathbf{M}^c_{\mathbf{x}\mathbf{x}^T}(\langle c(\mathbf{x},t)\rangle)}{\partial t} = \frac{\partial \mathbf{M}_{\mathbf{x}\mathbf{x}^T}(\langle c(\mathbf{x},t)\rangle)}{\partial t} - \frac{\partial\left(\mathbf{m}_{\mathbf{x}}(\langle c(\mathbf{x},t)\rangle)\mathbf{m}_{\mathbf{x}}^T(\langle c(\mathbf{x},t)\rangle)\right)}{\partial t} \quad \text{(A7)}$$

$$\frac{\partial \langle \mathbf{M}^c_{\mathbf{x}\mathbf{x}^T}(c(\mathbf{x},t))\rangle}{\partial t} = \frac{\partial \mathbf{M}^c_{\mathbf{x}\mathbf{x}^T}(\langle c(\mathbf{x},t)\rangle)}{\partial t} - \frac{\partial \langle \mathbf{m}'_{\mathbf{x}}(c(\mathbf{x},t))\mathbf{m}'^T_{\mathbf{x}}(c(\mathbf{x},t))\rangle}{\partial t} \quad \text{(A8)}$$

Appendix B: Steps in the Derivation of Closed-Form Solutions

B1. Mixed Contribution to Transverse Macrodispersion $D^*_{mix,22}(t)$

[63] Using dimensionless variables, the term to be evaluated is:

$$\frac{D^*_{mix,22}(t^*)}{\sigma_Y^2\langle v_1\rangle\lambda} = 2J^{*2}\int_0^{t^*}(\exp(2\pi i\omega^*\tau)+\exp(-2\pi i\omega^*\tau^*)) \cdot \int_{\infty} \exp(-4\pi\mathbf{s}^T\mathbf{s})\left(1-\frac{s_2^2}{\mathbf{s}^T\mathbf{s}}\right)^2 \cdot \exp(2\pi i s_1\tau^* - 4\pi^2\varepsilon\mathbf{s}^T\mathbf{s}\tau^*)\cdot d\mathbf{s}d\tau^* \quad \text{(B1)}$$

in which we have expressed the cosine function by its corresponding complex exponential form. The derivation of closed-form expressions is based on the following steps.

[64] 1. Integration over the Fourier variables s_1, s_2, s_3. Here we replace the fractions $1/(\mathbf{s}^T\mathbf{s})$ by the following identities:

$$\frac{1}{\mathbf{s}^T\mathbf{s}} = 4\pi\int_0^{\infty}\exp(-4\pi\mathbf{s}^T\mathbf{s}\tau')d\tau' \quad \text{(B2)}$$

$$\frac{1}{(\mathbf{s}^T\mathbf{s})^2} = 16\pi^2\int_0^{\infty}\tau'\exp(-4\pi\mathbf{s}^T\mathbf{s}\tau')d\tau' \quad \text{(B3)}$$

[65] 2. Expansion of the integrand with respect to small inverse Peclet numbers. In order to achieve this goal, we expand the integrand about ϵ τ^*. Afterward,we perform the integration over the dimensionless time variable τ^*.

[66] 3. Integration over the auxiliary variable τ'. In order to perform this integration in closed-form, we need to expand

$$\operatorname{erf}\left(\frac{\tau^* - \pi^2 i\omega^*\left(\frac{4+4\tau'}{\pi}\right)}{\sqrt{\frac{4+4\tau'}{\pi}}}\right) - \operatorname{erf}\left(\frac{\tau^* + \pi^2 i\omega^*\left(\frac{4+4\tau'}{\pi}\right)}{\sqrt{\frac{4+4\tau'}{\pi}}}\right) \quad \text{(B4)}$$

about $\tau' = 0$. The correction terms vanish exponentially fast according to $\exp(-t^*)$.

B2. Mixed Contribution to Transverse Effective Dispersion $D^e_{mix,22}(t)$

[67] Using dimensionless variables, the term to be evaluated is:

$$\frac{D^e_{mix,22}(t)}{\sigma_Y^2\lambda\langle v_1\rangle} = \frac{D^*_{mix,22}(t)}{\sigma_Y^2\lambda\langle v_1\rangle} - 2J^{*2}\int_0^{t^*}(\exp(2\pi i\omega^*\tau)+\exp(-2\pi i\omega^*\tau^*)) \cdot \int_{\infty}\exp(-4\pi\mathbf{s}^T\mathbf{s})\left(1-\frac{s_2^2}{\mathbf{s}^T\mathbf{s}}\right)^2 \cdot \exp(2\pi i s_1\tau^* + 4\pi^2\varepsilon(\tau^*-2t^*)\mathbf{s}^T\mathbf{s})d\mathbf{s}d\tau^* \quad \text{(B5)}$$

[68] The leading order behavior of the second term can be derived by rescaling the integration variables and dimensionless parameters.

$$\mathbf{s} \longrightarrow \mathbf{s}\sqrt{1+2\pi\varepsilon t^*} \quad \text{(B6)}$$

$$\tau \longrightarrow \tau/\sqrt{1+2\pi\varepsilon t^*} \quad \text{(B7)}$$

$$t^* \longrightarrow t^*/\sqrt{1+2\pi\varepsilon t^*} \quad \text{(B8)}$$

$$\omega^* \longrightarrow \omega^*\sqrt{1+2\pi\varepsilon t^*} \quad \text{(B9)}$$

[69] For $\exp(-4\pi^2\varepsilon\tau\mathbf{s}^T\mathbf{s})$, we write $\exp(-4\pi^2\varepsilon^*\tau\mathbf{s}^T\mathbf{s})$ with $\varepsilon^* \equiv \varepsilon/\sqrt{1+2\pi\varepsilon t^*}$. The rescaling yields the factor $1/(1+2\pi t^*)$ in front of the integral. The remaining integral

equals $D^*_{mix,22}(t)$ with rescaled variables. The evaluation of the integrations follows the scheme outlined above.

Appendix C: Approximation by the Discrete Fourier Transformation

[70] In equations (31) and (32), the macrodispersion and effective dispersion coefficients, $\mathbf{D}^*(t)$ and $\mathbf{D}^e(t)$, are given as functions of the velocity spectrum/covariance $\mathcal{S}_{\mathbf{v}'\mathbf{v}''}(\mathbf{s},\tau)$, defined in equation (20). Here we obtain a numerical approximation for a periodic field by application of fast Fourier transformation (FFT) techniques. Consider a three-dimensional unit cell discretized by $n_1 \times n_2 \times n_3$ grid points with index $\mathbf{j} = [j_1, j_2, j_3]^T$. The corresponding discrete Fourier transform $\hat{f}(\mathbf{k})$ has the same number of grid points with the index $\mathbf{k} = [k_1, k_2, k_3]^T$. Then the operation of the discrete Fourier transformation $\mathcal{F}(f(\mathbf{J}))$ and its inverse $\mathcal{F}^{-1}(\hat{f}(\mathbf{k}))$ is defined as (see chapter 12 of [*Press et al.*, 1992]):

$$\hat{f}(\mathbf{k}) = \mathcal{F}(f(\mathbf{j})) = \sum_{j_1=0}^{n_1-1}\sum_{j_2=0}^{n_2-1}\sum_{j_3=0}^{n_3-1} f(j_1,j_2,j_3) \cdot \exp\left(-\frac{2\pi i(j_1k_1 + j_2k_2 + j_3k_3)}{n_1n_3n_3}\right) \tag{C1}$$

$$f(\mathbf{j}) = \mathcal{F}^{-1}(\hat{f}(\mathbf{k})) = \frac{1}{n_1n_2n_3}\sum_{k_1=0}^{n_1-1}\sum_{k_2=0}^{n_2-1}\sum_{k_3=0}^{n_3-1} \hat{f}(k_1,k_2,k_3) \cdot \exp\left(\frac{2\pi i(j_1k_1 + j_2k_2 + j_3k_3)}{n_1n_3n_3}\right) \tag{C2}$$

in which we have chosen to start the indices at zero. For given indices $\mathbf{j}$ and $\mathbf{k}$, the spatial coordinate $\mathbf{x}(\mathbf{j})$ for a unit cell centered about the origin, the wave number $\mathbf{s}(\mathbf{k})$, and the corresponding Fourier transform $\tilde{f}(\mathbf{s}(\mathbf{k}))$ of the continuous function $f(\mathbf{x})$ are given by:

$$\mathbf{x}(\mathbf{j}) = \begin{bmatrix} \left(\frac{j_1}{n_1} - \frac{n_1}{2}\right)L_1 \\ \left(\frac{j_2}{n_2} - \frac{n_2}{2}\right)L_2 \\ \left(\frac{j_3}{n_3} - \frac{n_3}{2}\right)L_3 \end{bmatrix}, \mathbf{s}(\mathbf{k}) = \begin{bmatrix} \frac{k_1}{L_1} - \frac{n_1}{2L_1} \\ \frac{k_2}{L_2} - \frac{n_2}{2L_2} \\ \frac{k_3}{L_3} - \frac{n_3}{2L_3} \end{bmatrix}, \quad \tilde{f}(\mathbf{s}(\mathbf{k})) = \frac{L_1L_2L_3}{n_1n_2n_3}\hat{f}(\mathbf{k}) \tag{C3}$$

while the integration over the spectral domain becomes:

$$\int_{\infty} \tilde{f}(\mathbf{s})d\mathbf{s} = \frac{1}{n_1n_2n_3}\sum_{k_1=0}^{n_1-1}\sum_{k_2=0}^{n_2-1}\sum_{k_3=0}^{n_3-1} \hat{f}(k_1,k_2,k_3) \tag{C4}$$

[71] With these identities, the dispersion coefficients obtained from first-order stochastic theory are approximated by the following procedure.

[72] 1. The covariance function $R_{Y'Y(\mathbf{h})}$ of log conductivity is calculated for all grid points belonging to a unit cell centered about the origin. To ensure that the covariance function is even, the discretized covariance function $R_{Y'Y}(\mathbf{J})$ is shifted such that the variance appears at node 0, 0, 0 rather than the center node. The discrete Fourier spectrum $\hat{S}_{Y'Y}(\mathbf{k})$ is obtained by FFT (equivalent to equation (C1)). $\hat{S}_{YY}(\mathbf{0})$ is set to zero to ensure that the mean of the fluctuations is zero.

[73] 2. The vector of wave numbers $\mathbf{s}(\mathbf{k})$ is calculated according to equation (C3) for each node of the spectral domain. The discrete spatial spectrum/temporal covariance $\hat{S}_{\mathbf{q}'\mathbf{q}''}(\mathbf{k}, \tau)$ of the specific discharge components is calculated node-wise for each time-lag τ according to equation (20) using $\hat{S}_{Y'Y}(\mathbf{k})$ rather than $S_{Y'Y}(\mathbf{s}(\mathbf{k}))$. The discrete spectrum/covariance $\hat{S}_{\mathbf{v}'\mathbf{v}''}(\mathbf{k}, \tau)$ = of the seepage velocity is then substituted node-wise into equations (31) and (32).

[74] 3. The integration over the spectral domain in equations (31) and (32) is replaced by summation over all nodes and division by the total number of nodes. For integration in time, the midpoint rule is applied.

[75] The integrands in the temporal integration of equations (31) and (32) do not depend on the time t for which $\mathbf{D}^*(t)$ and $\mathbf{D}^e(t)$ are to be evaluated. The time t appears only as the upper integration limit and, in equation (32), in a factor outside of the temporal integral. This makes the evaluation of $\mathbf{D}^*(t)$ and $\mathbf{D}^e(t)$ at different times computationally efficient. Given the macrodispersion tensor $\mathbf{D}^*(t_1)$ at time t_1, the evaluation of the tensor at a later time t_2 requires only temporal integration from t_1 to t_2. This is different for the evaluation of $\mathbf{D}^*(t)$ and $\mathbf{D}^e(t)$ assuming deterministic fluctuations of the mean head gradient $\mathbf{J}(t)$. The temporal integrand in equations (52) and (53) depends via the mean displacement $\langle \mathbf{x}(t) \rangle$ on the limit t of the integral. The corresponding evaluation of $\mathbf{D}^*(t)$ and $\mathbf{D}^e(t)$ at any given time t requires performing the full integration from zero to t, even if the dispersion tensors have been evaluated for previous times.

[76] All numerical procedures are written as Matlab scripts, in which indices start at one rather than zero. The implementation of the discrete Fourier transform within Matlab is based on the FFTW-library (http://www.fftw.org) which allows any number of points per direction rather than a power of two, as required by standard FFT.

[77] **Acknowledgments.** Funding for this research is provided by the Emmy-Noether program of the Deutsche Forschungsgemeinschaft under the grant Ci-26/3-3. The authors thank Wolfgang Nowak for reviewing a draft of the manuscript and two anonymous reviewers helping to improve the quality of the paper.

References

Abramowitz, M., and I. A. Stegun (Eds.), *Handbook of Mathematical Functions*, Dover, Mineola, N.Y., 1974.

Andricevic, R., and V. Cvetkovic, Relative dispersion for solute flux in aquifers, *J. Fluid Mech.*, *361*, 145–174, 1998.

Attinger, S., M. Dentz, H. Kinzelbach, and W. Kinzelbach, Temporal behaviour of a solute cloud in a chemically heterogeneous porous medium, *J. Fluid Mech.*, *386*, 77–104, 1999.

Bellin, A., G. Dagan, and Y. Rubin, The impact of head gradient transients on transport in heterogeneous formations: Application to the Borden site, *Water Resour. Res.*, *32*, 2705–2713, 1996.

Chatwin, P., and P. Sullivan, Relative diffusion of a cloud of passive contaminant in incompressible turbulent flow, *J. Fluid Mech.*, *91*, 225–337, 1979.

Cirpka, O., Choice of dispersion coefficients in reactive transport calculations on smoothed fields, *J. Contam. Hydrol.*, *58*, 261–282, 2002.

Cirpka, O. A., and P. K. Kitanidis, An advective-dispersive stream tube approach for the transfer of conservative tracer data to reactive transport, *Water Resour. Res.*, *36*, 1209–1220, 2000.

Cirpka, O. A., E. O. Frind, and R. Helmig, Numerical simulation of biodegradation controlled by transverse mixing, *J. Contam. Hydrol.*, *40*, 159–182, 1999.

Dagan, G., Time-dependent macrodispersion for solute transport in anisotropic heterogeneous aquifers, *Water Resour. Res.*, *24*, 1491–1500, 1988.

Dagan, G., A. Bellin, and Y. Rubin, Lagrangian analysis of transport in heterogeneous formations under transient flow conditions, *Water Resour. Res.*, *32*, 891–899, 1996.

Dentz, M., Temporal behavior of transport parameters in heterogeneous porous media, Ph.D., thesis, Fak. für Phys., Univ. Heidelberg, Heidelberg, Germany, 2000.

Dentz, M., H. Kinzelbach, S. Attinger, and W. Kinzelbach, Temporal behavior of a solute cloud in a heterogeneous porous medium: 1. Point-like injection, *Water Resour. Res.*, *36*, 3591–3604, 2000a.

Dentz, M., H. Kinzelbach, S. Attinger, and W. Kinzelbach, Temporal behavior of a solute cloud in a heterogeneous porous medium: 2. Spatially extended injection, *Water Resour. Res.*, *36*, 3605–3614, 2000b.

Dykaar, B. B., and P. K. Kitanidis, Determination of the effective hydraulic conductivity for heterogeneous porous media using a numerical spectral approach: 1. Method, *Water Resour. Res.*, *28*, 1155–1166, 1992.

Fiori, A., The relative dispersion and mixing of passive solutes in transport in geologic media, *Transp. Porous Media*, *42*, 69–83, 2001.

Fiori, A., and G. Dagan, Concentration fluctuations in aquifer transport: A rigorous first-order solution and applications, *J. Contam. Hydrol.*, *45*, 139–163, 2000.

Gelhar, L. W., *Stochastic Subsurface Hydrology*, Prentice-Hall, Old Tappan, N.J., 1993.

Gelhar, L. W., and C. L. Axness, Three-dimensional stochastic analysis of macrodispersion in aquifers, *Water Resour. Res.*, *19*, 161–180, 1983.

Goode, D., and L. Konikow, Apparent dispersion in transient groundwater flow, *Water Resour. Res.*, *26*, 2339–2351, 1990.

Indelman, P., and Y. Rubin, Solute transport in nonstationary velocity fields, *Water Resour. Res.*, *32*, 1259–1267, 1996.

Kabala, Z., and G. Sposito, A stochastic model of reactive solute transport with time-varying velocity in a heterogeneous aquifer, *Water Resour. Res.*, *27*, 341–350, 1991.

Kavvas, M., and A. Karakas, On the stochastic theory of solute transport by unsteady and steady groundwater flow in heterogeneous aquifers., *J. Hydrol.*, *179*, 321–351, 1996.

Kinzelbach, W., and P. Ackerer, Modelisation de la propagation d'un contaminant dans un champ d'ecoulement transitoire, *Hydrogeologie*, *2*, 197–205, 1986.

Kitanidis, P. K., Prediction by the method of moments of transport in heterogeneous formations, *J. Hydrol.*, *102*, 453–473, 1988.

Kitanidis, P. K., Analysis of macrodispersion through volume-averaging: Moment equations, *Stochastic Hydrol. Hydraul.*, *6*, 5–25, 1992.

Klenk, I., and P. Grathwohl, Transverse vertical dispersion in groundwater and the capillary fringe, *J. Contam. Hydrol.*, *58*, 111–128, 2002.

Li, L., and W. Graham, Stochastic analysis of solute transport in heterogeneous aquifers subject to spatiotemporal random recharge, *Water Resour. Res.*, *35*, 953–971, 1999.

Pollock, D. W., Semianalytical computation of path lines for finite-difference models, *Ground Water*, *26*, 743–750, 1988.

Press, W., S. Teukolsky, W. Vetterling, and B. Flannery, *Numerical Recipes in FORTRAN 77: The Art of Scientific Computation*, 2nd ed., Cambridge Univ. Press, New York, 1992.

Rajaram, H., and L. W. Gelhar, Plume scale-dependent dispersion in heterogeneous aquifers: 2. Eulerian analysis and three-dimensional aquifers, *Water Resour. Res.*, *29*, 3261–3276, 1993.

Rajaram, H., and L. W. Gelhar, Plume-scale dispersion in aquifers with a wide range of scales of heterogeneity, *Water Resour. Res.*, *31*, 2469–2482, 1995.

Rehfeldt, K. R., and L. W. Gelhar, Stochastic analysis of dispersion in unsteady flow in heterogeneous aquifers, *Water Resour. Res.*, *28*, 2085–2099, 1992.

Ruge, J., and K. Stüben, Algebraic multigrid (AMG), in *Multigrid Methods, Frontiers Appl. Math.*, vol. 3, edited by S. F. McCormick, pp. 73–130, Soc. for Indust. and Appl. Math., Philadelphia, Pa., 1987.

Schirmer, M., G. C. Durrant, J. W. Molson, and E. O. Frind, Influence of transient flow on contaminant biodegradation, *Ground Water*, *39*, 276–282, 2001.

Thornton, S., S. Quigley, M. Spence, S. Banwart, S. Bottrell, and D. Lerner, Processes controlling the distribution and natural attenuation of dissolved phenolic compounds in a deep sandstone aquifer, *J. Contam. Hydrol.*, *53*, 233–267, 2001.

Thullner, M., L. Mauclaire, M. Schroth, W. Kinzelbach, and J. Zeyer, Interaction between water flow and spatial distribution of microbial growth in a two-dimensional flow field in saturated porous media, *J. Contam. Hydrol.*, *58*, 169–189, 2002.

Wood, B., and M. Kavvas, Ensemble-averaged equations for reactive transport in porous media under unsteady flow conditions, *Water Resour. Res.*, *35*, 2053–2068, 1999.

Woodbury, A., and E. Sudicky, The geostatistical characteristics of the Borden aquifer, *Water Resour. Res.*, *27*, 533–546, 1991.

Zhang, D., Numerical solutions to statistical moment equations of groundwater flow in nonstationary, bounded, heterogeneous media, *Water Resour. Res.*, *34*, 529–538, 1998.

Zhang, D., and S. Neuman, Head and velocity covariances under quasi-steady state flow and their effects on advective transport, *Water Resour. Res.*, *32*, 77–83, 1996.

Zhang, D., R. Andricevic, A. Y. Sun, X. Hu, and G. He, Solute flux approach to transport through spatially nonstationary flow in porous media, *Water Resour. Res.*, *36*, 2107–2120, 2000.

S. Attinger, Computational Science and Engineering, Swiss Federal Institute of Technology Zürich, Weinbergstrasse 43, 8092 Zürich, Switzerland. (sabine.attinger@inf.ethz.ch)

O. A. Cirpka, Institut für Wasserbau, Universität Stuttgart, Pfaffenwaldring 61, 70550 Stuttgart, Germany. (olaf.cirpka@iws.uni-stuttgart.de)